PCCP

Accepted Manuscript

ROYAL SOCIETY OF CHEMISTRY

www.rsc.org/pccp

Thursday, August 14, 2014

Title :

Introducing Asymmetry in Tetradentate Azadipyrromethene Chromophores: A Systematic Study of the Impact on Electronic and Photophysical Properties

*André Bessette[1,2], Mihaela Cibian[1], Francis Bélanger[2], Denis Désilets[2] and Garry S. Hanan[1] *.*

[1] Département de Chimie, Université de Montréal, Pavillon J.-A. Bombardier, 5155 Decelles Avenue, Montréal, Québec, H3T-2B1, Canada

[2] Saint-Jean Photochemicals Inc., 725 Trotter street, Saint-Jean-sur-Richelieu, Québec, J3B 8J8, Canada.

RECEIVED DATE (automatically inserted by publisher);

ABSTRACT

As analogues of the porphyrinoid and dipyrromethene families of dye, azadipyrromethene (ADPM) derivatives exhibit exciting photophysical properties. Their high absorbance (**ε** up to 100 000 $M^{-1}cm^{-1}$) in the yellow-to-red region and the strong NIR luminescence encountered in boron-chelated Aza-BODIPY analogues are especially interesting in the context of light-harvesting and life science applications. In the present study, we endeavored a comparative study of symmetric and asymmetric tetradentate ADPM derivatives **1** – **6** versus the reference bidentate motifs of **7** and **8** in order to gain insights on their structure – property relationship. This is of interest since the tetradentate motif opens the way for extended π-conjugation through metal-mediated planarization, in a bio-mimicry fashion of metalloporphyrinoids, and is known to induce a bathochromic shift toward the NIR. A new straightforward synthetic approach is used to access asymmetric derivatives **4** – **6** that avoids the tedious heterocycle formation of nitroso-pyrrole intermediates. In addition, photophysic, electrochemistry, computational modelization (DFT and TD-DFT) and X-ray structural characterization of ADPMs are used to better understand the potential of these new chromophores.

KEYWORDS

Azadipyrromethene; Panchromatic dyes; Tetradentate ligand design; Asymmetric synthesis; Heterocyclic synthesis; Photophysic; Electrochemistry; Computational modelization; DFT; TD-DFT; X-ray Structures.

INTRODUCTION

Azadipyrromethene (ADPM) is a class of deep blue organic chromophores discovered by Rogers[1] in the 1940's currently attracting renewed interest for its far-red to near-infrared (NIR) optical properties advantageously similar to dipyrromethene (DPM) and porphyrinoid (*e.g.* naturally-encountered Chlorophyll *a* chromophores) (Figure 1).[2] ADPM and DPM present the synthetic benefit of avoiding the low-yield macrocyclization step and difficult purification associated with porphyrinoids, while maintaining an intense absorption band (ε up to 100 000 $M^{-1}cm^{-1}$) in the yellow-to-red part of the spectrum. They also offer abundant leverage possibilities in order to fine-tune their properties by substituent modification and greater versatility of metal coordination geometries as compared to the rigid square-planar geometry encountered in tetrapyrrole macrocycles. The main advantage of ADPM over DPM resides in the intrinsic bathochromic shift in the absorption band (about 50 nm) provided by substitution to a nitrogen bridge at the *meso*- position of the DPM core. All these advantages coupled with the strong NIR emission in corresponding BF_2-chelates of DPM and ADPM, known in literature as BODIPY and Aza-BODIPY respectively, have led to a wide range of applications, including: fluorescent indicators and sensors;[3] fluorescence imaging agents;[4] photosensitizers for photodynamic therapy;[5] advanced luminescent and light-active material component;[6] nonlinear optic;[7] light-harvesting antennae[8] and photovoltaic devices.[2a, 9] With these multiple applications and their imperative need for further fine-tuning of optical and electrochemical properties, one field in which ADPM is actively used is coordination chemistry, where the metallic center opens up many new exciting opportunities.[9c, 10]

Figure 1 – Azadipyrromethene (ADPM) and dipyrromethene (DPM) cores along with Chlorophyll *a* porphyrin

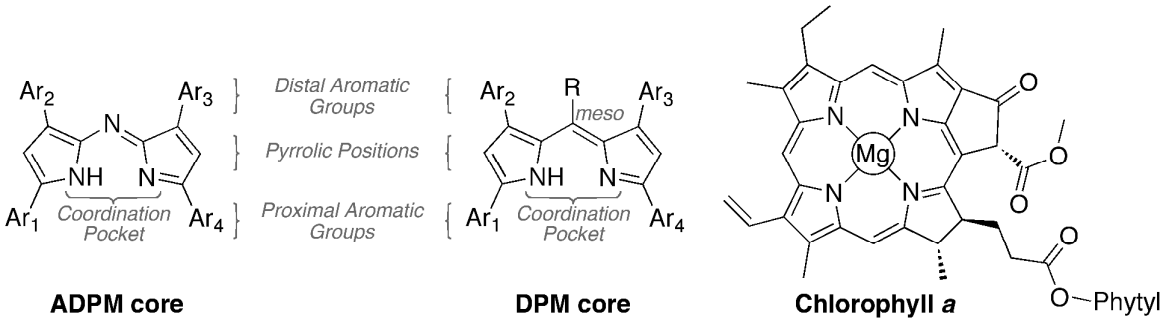

In this context, we are interested in the design of new ADPM that would coordinate metallic centers in a tetradentate fashion, red-shifting even further the NIR properties by extension of the conjugation. The concept of restricting the possible conformations of ADPM to induce a bathochromic shift in the spectral absorption and emission has already been demonstrated, either by ring constrain / fusion[11] or B-O chelation.[12] Toward this goal, metal-mediated planarization effects still need to be explored in a similar fashion as the bio-mimicry of metalloporphyrinoids and natural bilin-type chlorophyll catabolite metal complexes.[13] Applications other than light-harvesting and photovoltaic can further be envisioned for such derivatives, such as catalytic and biomedical ones.[14]

In order to achieve these organometallic structures, new symmetric and asymmetric tetradentate ADPM containing additional heterocycles or heteroatoms on the proximal aryl groups needs to be developed (refer to Figure 1). While thiophene and pyridine rings have already been used as replacement for phenyls,[3c, 15] their incorporation into a tetradentate motif was not optimal since the thiophenes lead to an overly wide bite angle for metallic coordination and the pyridines were reported only at the distal positions. In light of a recent mechanistic studies on the formation of tetraphenyl ADPM **7** using ^{15}N-labeling method reported by O'Shea

et al.,[16] we endeavored to investigate symmetric tetradentate ADPM **1** – **3** and their corresponding asymmetric analogues **4** – **6** (Figure 2). While asymmetric tetraaryl ADPMs were already accessible by condensation of 2,4-diaryl-5-nitroso-pyrroles with 2,4-diarylpyrroles,[11a, 17] we report herein a more straightforward synthesis that avoids tedious heterocycle formation of nitroso-pyrrole intermediates.[18] Our approach simply react the 2,4-diarylpyrrole with the easily accessible corresponding nitro-ketone precursor common to all ADPM dye formation. In addition to the new synthetic route proposed, a comparative study of the symmetric and asymmetric ADPM **1** – **8** including photophysic, electrochemistry, computational modelization (DFT and TD-DFT) and X-ray structural data analysis (for compounds **1**, **3**–**5** and **8**) will be presented in order to establish the trends and impact of the various accessible proximal aryl substitutions.

Figure 2 – ADPM compounds investigated herein.

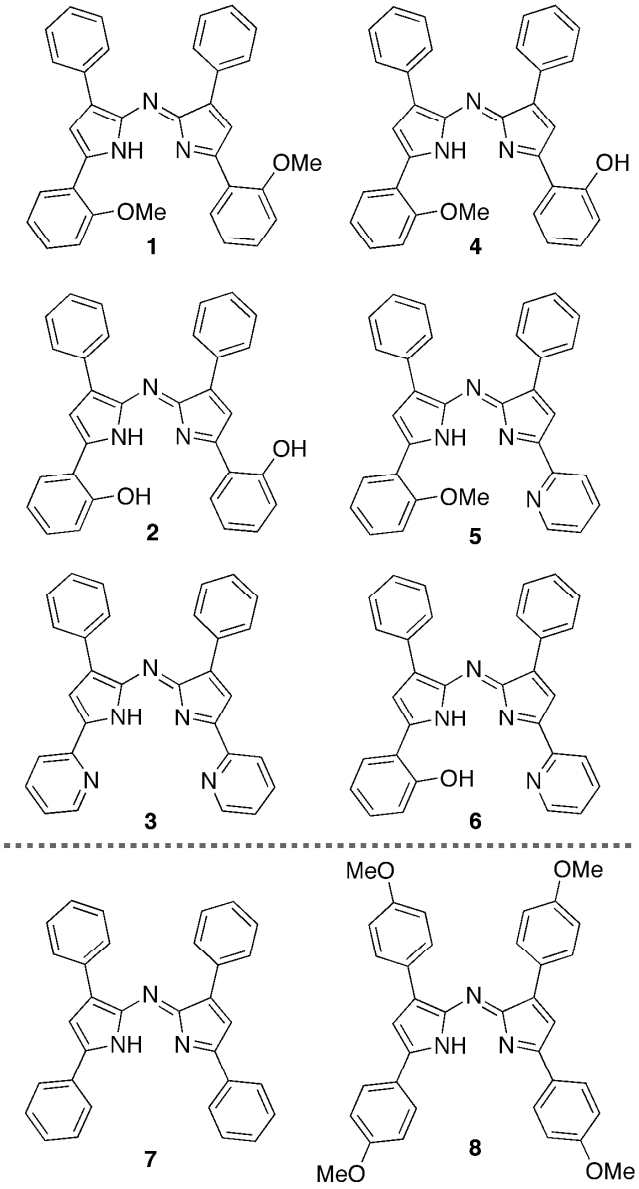

EXPERIMENTAL SECTION

Materials and Instrumentation

Literature procedures were used for the synthesis of compounds **1**, **2**, **7**, **10**, **11** and 3-phenyl-1-(pyridin-2-yl)prop-2-en-1-one.[5c, 11a, 12, 19] ADPM **8** was obtained from Saint-Jean Photochemicals Inc. (sjpc.com) and used as received. Reagents and solvents were obtained commercially and used without further purification. Reactions were carried out under ambient atmosphere. Solvents were removed under reduced pressure using a rotary evaporator unless otherwise stated.

Nuclear magnetic resonance (NMR) spectra were recorded in $CDCl_3$ at room temperature (r.t.) on a Bruker AV400 spectrometer at 400 MHz for ^{1}H NMR and at 100 MHz for ^{13}C NMR, unless otherwise stated. 125 MHz ^{13}C NMR of ADPM **4** was recorded on a Bruker Avance 500 spectrometer, while 175 MHz ^{13}C NMR of ADPM **5** and **6** were obtained on a Bruker Avance 700. Chemical shifts are reported in part per million (ppm) relative to residual solvent protons (7.26 ppm for chloroform-d) and the carbon resonance of the solvent (77.16 ppm for chloroform-d). High-Resolution Electro Spray Ionization Mass Spectrometry (HR-ESIMS) was performed on a Liquid Chromatography / Mass Spectrometry with a Time of Flight detector (LC/MS TOF) from Agilent. Absorption spectra were measured in CH_2Cl_2 (DCM) at concentrations obeying Beer-Lambert's law at r.t. on a Cary 500i UV-vis-NIR Spectrophotometer. The absence of fluorescence for the series of ADPM investigated herein was assessed on a Cary Eclipse Fluorescence Spectrophotometer. Full details on crystal structure determination and refinement data for compounds **1**, **3**, **4** and **5** are provided in Supporting Information (SI).

Electrochemical measurements were carried out in argon-purged CH_2Cl_2 at room temperature with a BAS CV50W multipurpose potentiostat. The working electrode used was a glassy carbon electrode for every compound. The counter electrode was a Pt wire, and the pseudo-reference

electrode was a silver wire. The reference was set using an internal 1 mM ferrocene/ferrocenium sample at 0.46 V vs SCE in CH_2Cl_2. The concentration of the compounds was about 1 mM. Tetrabutylammonium hexafluorophosphate (TBAP) was used as supporting electrolyte and its concentration was 0.10 M. Cyclic voltammograms (CV) were obtained at scan rates of 50, 100, 200, and 500 mV/s. For reversible processes, half-wave potentials (vs. SCE) from CV were used. To establish the potential of irreversible processes, differential pulse voltammetry (DPV) experiments were performed with a step rate of 4 mV, a pulse height of 50 mV, and a frequency of 5 Hz. Criteria for reversibility were the separation of 60 mV between cathodic and anodic peaks, the close to unity ratio of the intensities of the cathodic and anodic currents, and the constancy of the peak potential on changing scan rate.

Experimental uncertainties are as follows: absorption maxima, ±2 nm; molar absorption coefficient, 10%; redox potentials, ± 10 mV.

Computational Methods

Computational modelization of ADPM **1** – **8** was achieved following the general procedure depicted by Jacquemin and coworkers for Aza-BODIPYs.[20] All calculations were performed with the Gaussian 09 software (G09).[21] Geometry optimizations, frequency calculations and molecular orbital (MO) calculations were performed by DFT method using the PBE0[22] / 6-311G(2d,p) basis set using the Polarization Continuum Model (PCM)[23] of dichloromethane. Crystallographic coordinates were used as starting points for geometry optimizations when available. When no crystallographic data were available for a given compound, modification of a similar derivative was used. Tight convergence criteria and no symmetry constraints were imposed during the optimization process. Only positive frequencies were found for the optimized structures. The absorption spectra were calculated by TD-DFT from optimized structures, using the BMK[24] / 6-

311+G(2d,p) level of theory with the PCM of dichloromethane. MOs were visualized (isovalue = 0.02) with GaussView 3 software.[25] GaussSum 6.5 was employed to extract from TD-DFT results the absorption energies and oscillator strengths, while molecular orbital energies were obtained from DFT.[26] Chemissian 3.3 program was used to represent MO's energy levels (Figure 5), experimental vs calculated optical absorption spectrum (refer to SI) and determine the electronic distribution (in %) of the various parts of the ADPM chromophore (refer to SI).[27]

Synthetic Methods

Azadipyrromethene **3**

4-nitro-3-phenyl-1-(pyridin-2-yl)butan-1-one **9** (1.00 g, 3.70 mmol) was dissolved in EtOH (3 mL) and ammonium acetate (10.2 g, 130 mmol) was added and the reaction mixture was refluxed for 12 h. The reaction mixture was evaporated to dryness, dissolved in CH_2Cl_2 and washed with water (3x). The organic phase was evaporated and the purple residue was purified by silica gel chromatography (1 : 1 THF / heptane). The product crystallized as thin dark purple needles suitable for X-ray structural analysis on the sides of the collection tubes, while decomposition in solution occurs. Yield = 9 mg (1 %). ^{1}H NMR ($CDCl_3$, 400 MHz) δ/ppm: 7.26 (br. s., 1 H), 7.30 - 7.54 (m, 10 H), 7.81 - 7.90 (m, 2 H), 8.09 (d, *J*=7.3 Hz, 3 H), 8.22 (br. s., 2 H), 8.77 (d, *J*=4.0 Hz, 2 H), 12.79 (br. s., 1 H). Mass Spec (*m/z*); MS calcd for $C_{30}H_{21}N_5$: $[(M+H)^+]$ 452.18697, found: 452.18572.

Azadipyrromethene **4**

A suspension of 2-(2-methoxyphenyl)-4-phenyl-1*H*-pyrrole **10** (409 mg, 1.64 mmol) and 1-(2-hydroxyphenyl)-4-nitro-3-phenylbutan-1-one **11** (444 mg, 1.64 mmol) in EtOH (5 mL) was heated to 50 °C under magnetic stirring. Upon solubilization, ammonium acetate (4.52 g, 57.3 mmol) was added and the reaction mixture was refluxed for 24 h. The crude mixture was cooled

down, evaporated to dryness, dissolved in CH_2Cl_2 and washed with water (3x). The organic phase was evaporated and the dark-purple residue was purified by silica gel chromatography (15 : 85 AcOEt / heptane). Recrystallization in hot heptane and *in vacuo* drying afforded dark purple needles suitable for X-ray structural analysis. Yield = 368 mg (45 %). ^{1}H NMR ($CDCl_3$, 400 MHz) δ/ppm: 4.04 (s, 3 H), 7.03 (t, *J*=7.6 Hz, 1 H), 7.06 - 7.17 (m, 4 H), 7.32 - 7.47 (m, 8 H), 7.48 (s, 1 H), 7.79 - 7.90 (m, 2H), 7.98 - 8.07 (m, 4 H), 11.41 (br. s., 1 H), 12.55 (s, 1 H). ^{13}C NMR ($CDCl_3$, 125 MHz) δ/ppm: 169.7, 160.6, 157.2, 148.3, 139.4, 136.4, 135.9, 134.0, 133.2, 133.1, 130.2, 129.6, 129.2, 128.9, 128.6, 128.2 (2C), 128.1, 127.7, 127.6, 121.3, 121.1, 119.6, 118.1, 117.3, 117.2, 111.9, 109.9, 56.6. Mass Spec (*m/z*); HR-ESIMS calcd for $C_{33}H_{25}N_3O_2$: $[(M+H)^+]$ 496.20195, found: 496.20238. Elemental Analysis: calcd: C = 79.98 %, H = 5.08 %, N = 8,48 %; found: C = 79.83 %, H = 5.00 %, N = 8.43 %.

Azadipyrromethene **5**

2-(2-methoxyphenyl)-4-phenyl-1*H*-pyrrole **10** (300 mg, 1.20 mmol) and 4-nitro-3-phenyl-1-(pyridin-2-yl)butan-1-one **9** (325 mg, 1.20 mmol) were dissolved in EtOH (5 mL). Ammonium acetate (590 mg, 7.44 mmol) was added and the reaction mixture was refluxed for 12h. The reaction mixture was evaporated to dryness, dissolved in CH_2Cl_2 and washed with water (3x). The organic phase was evaporated and the dark-blue residue was purified by silica gel chromatography (25 : 75 AcOEt / heptane). The dark-purple powder obtained was recrystallized with DCM and heptane to afford purple/gold-shinning cubic crystals suitable for X-ray structural analysis. Yield = 115 mg (40 %).^{1}H NMR ($CDCl_3$, 400 MHz) δ/ppm: 4.05 (s, 3 H), 7.09 (d, *J*=8.4 Hz, 1 H), 7.16 (t, *J*=7.4 Hz, 1 H), 7.31 - 7.44 (m, 9 H), 7.44 - 7.50 (m, 1 H), 7.61(s, 1 H), 7.82 - 7.89 (m, 1 H), 7.93 - 8.07 (m, 4 H), 8.12 - 8.24 (m, 1 H), 8.76 (d, *J*=4.8 Hz, 1 H), 12.63 (br. s., 1 H). ^{13}C NMR ($CDCl_3$, 175 MHz) δ/ppm: 158.0, 157.7, 151.8, 151.4, 151.1, 149.9, 146.7, 143.3, 140.8, 136.3, 134.0, 133.8, 131.3, 129.4, 129.2, 129.1, 128.19, 128.17, 127.83, 127.77, 123.7,

121.5, 121.4, 120.5, 116.9, 116.4, 112.2, 56.2. Mass Spec (*m/z*); HR-ESIMS calcd for $C_{32}H_{25}N_4O$: [$(M+H)^+$] 481.20229, found: 481.20252. Elemental Analysis: calcd: C = 79.98 %, H = 5.03 %, N = 11.66 %; found: C = 79.95 %, H = 5.04 %, N = 11.75 %.

Azadipyrromethene **6**

A suspension of 2-(4-phenyl-1H-pyrrol-2-yl)phenol **12** (839 mg, 3.57 mmol) and 4-nitro-3-phenyl-1-(pyridin-2-yl)butan-1-one **9** (964 mg, 3.57 mmol) in EtOH (10 mL) was heated to 50°C under magnetic stirring. Upon solubilization, ammonium acetate (9.82 g, 125 mmol) was added and the reaction mixture was refluxed for 12h. The crude mixture was evaporated to dryness, dissolved in CH_2Cl_2 and washed with water (3x). The organic phase was evaporated and the dark-purple residue was purified by silica gel chromatography (25 : 75 AcOEt / heptane). Vacuum drying afforded a dark-purple powder. Yield = 712 mg (43 %). ^{1}H NMR ($CDCl_3$, 400 MHz) δ/ppm: 7.03 (t, *J*=7.5 Hz, 1 H), 7.10 - 7.21 (m, 2 H), 7.24 (br. s., 1 H), 7.31 - 7.38 (m, 1 H), 7.38 - 7.50 (m, 6 H), 7.53(s, 1 H), 7.71 - 7.79 (m, 2 H), 7.82 (d, *J*=7.7 Hz, 1 H), 8.02 (t, *J*=7.0 Hz, 4 H), 8.76 (d, *J*=4.4 Hz, 1 H), 11.19 (br. s., 1 H), 12.54 (br. s., 1 H). ^{13}C NMR ($CDCl_3$, 175 MHz) δ/ppm: 134.4, 134.2, 134.00, 133.99, 132.6, 130.9, 130.80, 130.77, 130.4, 129.9, 129.3, 129.0, 128.9, 128.7, 128.27, 128.25, 128.1, 127.9, 127.8, 127.7, 127.5, 127.4, 127.3, 122.7, 119.7, 118.0, 117.9. Mass Spec (*m/z*); HR-ESIMS calcd for $C_{31}H_{22}N_4O$: [$(M+H)^+$] 467.18664, found: 467.18724. Elemental Analysis: calcd for $C_{31}H_{22}N_4O \bullet 0.5\ H_2O$: C = 78.30 %, H = 4.87 %, N = 11.78 %; found: C = 78.27 %, H = 4.47 %, N = 11.98 %.

4-nitro-3-phenyl-1-(pyridin-2-yl)butan-1-one **9**

3-phenyl-1-(pyridin-2-yl)prop-2-en-1-one (10.0 g, 47.8 mmol) and nitromethane (27.25 mL, 478 mmol) were dissolved in EtOH (150 mL). KOH powder (0.54 g, 9.56 mmol) was added under magnetic stirring and the reaction mixture was heated at 60 °C for 3 h. The crude was concentrated *in vacuo* and purified by silica gel chromatography (2 : 8 AcOEt / heptane). Vacuum drying afforded dark yellow oil. Yield = 10.8 g (84 %). Characterization matched previously reported literature.[28]

2-(4-phenyl-1H-pyrrol-2-yl)phenol **12**

To a flamed-dried flask equipped with a magnetic stirrer, 2-(2-methoxyphenyl)-4-phenyl-1*H*-pyrrole **10** (1.40 g, 5.62 mmol) was dissolved in anhydrous CH_2Cl_2 (200 mL). The reaction mixture was then degassed and kept under an inert atmosphere (N_2) at 0 °C. A solution of 1M BBr_3 in CH_2Cl_2 (28.1 mL, 28.1 mmol) was added dropwise and the reaction mixture was stirred at 0 °C for 15 min. The reaction mixture was than warmed to r.t. and stirred for another 24 h (or upon completion by TLC). The reaction was cooled back to 0 °C and quenched by slow addition of water. The organic and aqueous phases were separated and the latter was further dried with anhydrous Na_2SO_4, filtered and concentrated *in vacuo*. The crude oil was purified by silica gel chromatography (2 : 8 AcOEt / Heptane). Vacuum drying afforded dark yellow oil. Yield = 839 mg (64 %). This light and air sensitive product was brought to the next step without further characterization.

RESULTS AND DISCUSSION

Design strategy

Our study began by the synthesis of symmetric tetra-aryl ADPM derivatives based on the known reaction of 4-nitro-1,3-diarylbutan-1-ones with an ammonium source in ethanol.[16] The tetradentate ADPM **1** with methoxy- and **2** with hydroxyl- groups were synthetized according to the procedures reported by O'Shea *et al.*[12, 19a] In the case of ADPM **3** bearing 2-pyridyl proximal substituents, we adapted the synthesis of the corresponding ADPM with 2-pyridyl substituents installed in distal positions reported by Akkaya and coworkers.[3c] Nitro-ketone derivative **9** was reacted in the presence of an excess of NH_4OAc (Scheme 1) to lead to the expected tetradentate chromophore in poor yield (1 %). Although the reaction proceeded smoothly to give the desired product (by TLC analysis), the amount of recovered ADPM after purification on silica gel column was very small.[29] We postulate the degradation of the product during purification arises from the increased reactivity of the adjacent carbons of the N-bridge due to the conjugated electron-poor pyridine substituents. Luckily, we found X-ray quality crystals of ADPM **3** forming upon slow evaporation on the walls of the collected fractions that confirmed the accessibility of this tetradentate motif (refer to X-ray section, Figure 7). Based on previous work, we believe further complexation of a metal ion should allow for an overall stabilization avoiding such decomposition.[10a]

Scheme 1 – Synthesis of the symmetric ADPM **3**.

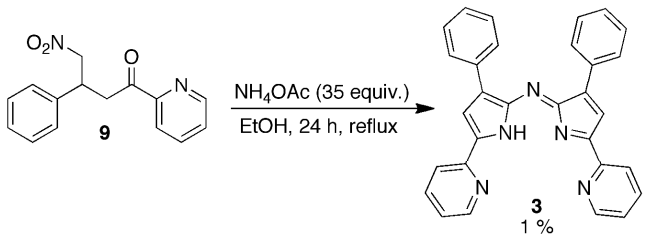

With symmetric tetradentate ADPM **1** – **3** in hand, we undertook the preparation of the more challenging asymmetric derivatives **4** – **6** in a combinatorial fashion. Our retrosynthetic analysis was based on the mechanistic insights provided lately by O'Shea and coworkers.[16] We envisioned that asymmetric tetraaryl ADPM could be obtained by reacting 2,4-diarylpyrrole with the corresponding nitro-ketone precursor common to the formation of all symmetric ADPM dyes. This new synthesis would avoid the tedious formation of nitroso-pyrrole intermediates[18] and open a straightforward route to asymmetric ADPMs. Indeed, one could envision obtaining a mixture of both symmetric products being obtained in addition to the desired asymmetric one. Keeping this challenge in mind, we were pleased to observe the selective formation of asymmetric ADPM **4** – **6** using our novel strategy (Scheme 2). Reaction conditions derived from the symmetric ADPM synthesis yielded the adduct **4** in a satisfactory 45% yield through the reaction for one day of 2-(2-methoxyphenyl)-4-phenyl-1*H*-pyrrole **10** with 1-(2-hydroxyphenyl)-4-nitro-3-phenylbutan-1-one **11** in the presence of ammonium acetate into ethanolic solution.[30] Using the same procedure, the 2,4-diarylpyrrole **10** was used with nitroketone **9** to access in 40% yield the ADPM **5** with a 2-methoxyphenyl and a 2-pyridyl as the proximal substituents. To obtain the 2-hydroxyphenyl / 2-pyridyl substituted ADPM **6**, a deprotection strategy of **10** using BBr_3 reagent to provide the intermediate 2-(4-phenyl-1*H*-pyrrol-2-yl)phenol **12** was used. This sensitive intermediate was quickly reacted after purification on silica column with 2-pyridyl nitroketone **9** to provide the

desired chromophore in 43% yield. It is noteworthy that our approach is the only one that gives access to this ADPM derivative. In fact, the 2-(4-phenyl-1*H*-pyrrol-2-yl)pyridine that would be needed in O'Shea's nitroso-pyrrole route is difficult to access since pyrrolic formation of the latter from nitroketone **9** was not possible. Similarly, the direct pyrrolic formation from the corresponding nitroketone **11** failed in our hands to yield **12**. Overall, the synthetic methodology presented herein to reach asymmetric tetradentate ADPMs present yields comparable to their corresponding symmetric derivatives in a forthright synthetic approach.

Scheme 2 – Synthesis of asymmetric ADPM derivatives **4** – **6**.

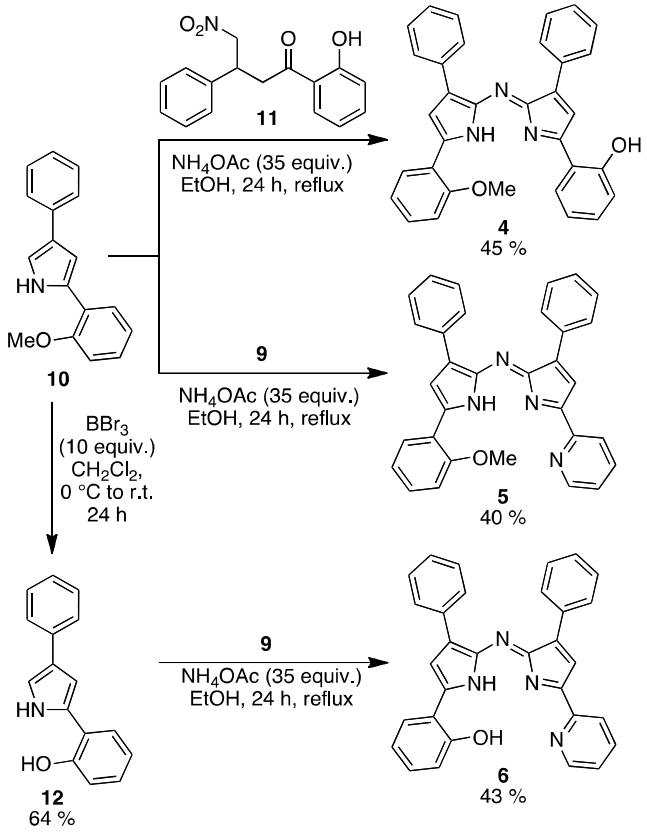

Spectroscopic Properties

The most attractive feature of azadipyrromethenes is their intense and broad absorption band found in the green to red part of the visible spectrum, leading to a purple / deep blue pigment. As mentioned previously, absorption at such low energy is of great interest for multiple applications and fine control on the exact wavelength of the maxima is therefore highly desirable. Spectroscopic properties in dichloromethane solution of tetradentate ADPMs **1** – **6** were recorded and are summarized in Table 1. No fluorescence was observed for the series. Further comparisons were made to related bidentate motif ADPM derivatives **7** and the more electron-rich **8,** previously reported bearing four *p*-methoxyphenyl substituents.[10a]

Table 1 – Compiled UV / vis absorption data for ADPM derivatives **1** – **8** in CH_2Cl_2 and corresponding TD-DFT calculated absorption band for $\lambda_{max\ red}$

	Absorption [a] [b]				Abs band [c]
	$\lambda_{max\ near\text{-}UV}$, nm	$\lambda_{max\ violet}$, nm	$\lambda_{shoulder}$, nm	$\lambda_{max\ red}$, nm	$\lambda_{max\ red\ Theo}$ nm
1	299 (34)	407 (6.8)	---	605 (47)	553 (0.834)
2	307 (26)	415 (6.0)	577 (21)	615 (39)	560 (0.834)
3	307 (30)	---	558 (28)	590 (39)	547 (0.877)
4	307 (35)	417 (8.3)	576 (28)	619 (52)	571 (0.861)
5	298 (30)	417 (3.9)	567 (24)	602 (33)	566 (0.830)
6	308 (36)	418 (6.9)	561 (28)	598 (43)	564 (0.850)
7	302 (41)	---	---	596 (46)	551 (0.885)
8	322 (40)	414 (10)	---	627 (52)	587 (0.889)

[a] Acquisition at 293K. [b] Extinction coefficient given in parenthesis (ε □□x10^3 $M^{-1}cm^{-1}$). [c] TD-BMK/6-311+G(2d,p); PCM = CH_2Cl_2. Oscillator strength given in parenthesis. Full assignation of the absorption bands available in SI (Tables S.2 – S.9)

For the symmetric tetradentate derivatives **1** – **3** (Figure 3a), ADPM **2** ($\lambda_{max\ red}$ = 615 nm) bearing *ortho*-hydroxyphenyl substituents in proximal position exhibits the highest bathochromic shift (+19 nm) compared to the reference ADPM **7** ($\lambda_{max\ red}$ = 596 nm). In contrast, ADPM **1** ($\lambda_{max\ red}$ = 605 nm) with methoxy groups presents a bathochromic shift of +9 nm. These red shifts

in the absorption maxima for ADPM **1** and **2** result from the contributions of electron-donors moieties, in a similar fashion to the +31 nm shift observed in the analogous ADPM **8**. Purely based on an analysis of the Hammett parameter, the biggest red shift arising from hydroxyl groups in ADPM **2** compared to methoxy groups in ADPM **1** (+19 nm vs +9 nm, respectively) is consistent with their relative electron-donating behavior (σ = -0.37 for -OH vs σ = -0.27 for -OMe).[31] In addition, the intramolecular H-bonds in dichloromethane solutions of ADPM **1** and **2** contribute to improve the overall conjugation throughout the molecules, thus leading to lower energy light absorption. This argument was first observed in the X-ray structure of ADPM **1** (see X-ray section; Figure 7), which was subsequently supported for both ADPM **1** and **2** by computational modelization with application of the Polarity Continuum Model (PCM) of dichloromethane (see Computational Modelization section). On the other hand, the electron deficient 2-pyridyl moieties in ADPM **3** ($\lambda_{max\ red}$ = 590 nm) provide a hypsochromic shift of -6 nm compared to ADPM **7**, also in accordance with the Hammett parameter argument (σ = 0.17 for 2-pyridyl moiety).[31] Interestingly, appearance of a small additional absorption band in the violet / blue at (~ 410 nm, ε = ~ 6 x 10^3 $M^{-1}cm^{-1}$) is noticeable for the two first tetradentate derivatives **1** and **2**, a behavior also found in the *p*-methoxy substituted ADPM **8**. As will be discussed in more details in the Computational Modelization section, TD-DFT calculations identified this absorption band as an electronic transition from the methoxy or hydroxyl groups toward the ADPM core. Overall, the symmetric tetradentate ADPM derivatives **1** – **3** reveal that a modulation of up to 25 nm is achievable ranging from the electron-poor ADPM **3** to the electron-richest ADPM **2**, which also takes advantage of intramolecular hydrogen bonding in the latter.

Figure 3 – Absorption spectra in DCM of: *a)* symmetric ADPM derivatives **1** – **3**, **7** and **8** *b)* asymmetric **4** – **6**.

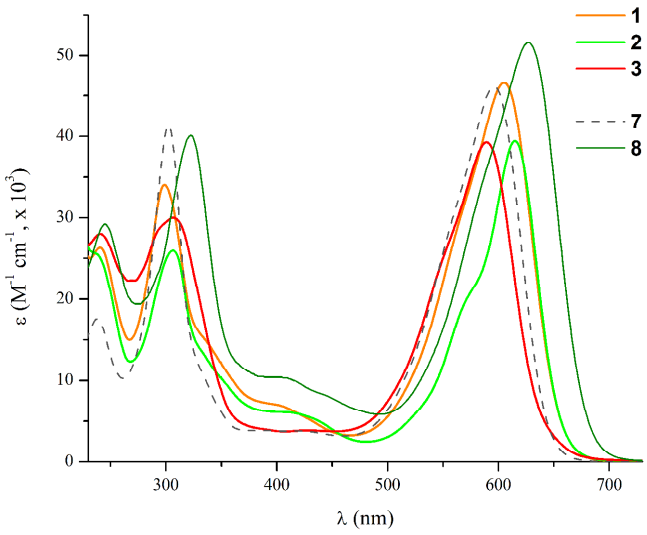

a)

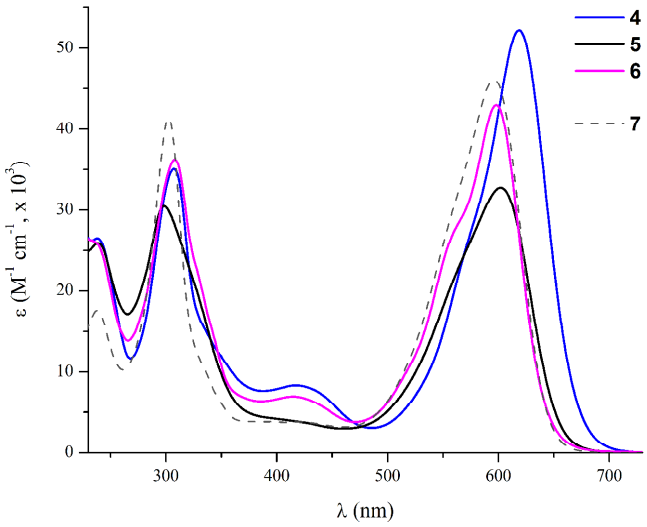

b)

Asymmetric tetradentate derivatives **4** – **6** (Figure 3b) present an advantageous combination of the properties observed in their symmetric counterparts. For instance, in the case of ADPM **4** the intramolecular H-bonds are acting in a synergetic manner to push the absorption up to 619 nm (+23 nm compared to ADPM **7**) (see X-ray section; Figure 8). Similarly, the extinction coefficient significantly increases as compared to the reference (ε □□□52 x 10^3 for **4** vs 46 x 10^3

$M^{-1}cm^{-1}$ for **7**). Remarkably, this synergy leads to planarization of the ADPM chromophore and a bathochromically-shifted intense absorption that gives good insight on the metal ion coordination effect. The integration of a 2-pyridyl moiety in ADPM **5** ($\lambda_{max\ red}$ = 602 nm) and **6** ($\lambda_{max\ red}$ = 598 nm) provides smaller bathochromic shifts of +6 and +2 nm, respectively. A decrease in extinction coefficients was also observed for **5** and **6** (ε □□□33 x 10^3 $M^{-1}cm^{-1}$ and 43 x 10^3 $M^{-1}cm^{-1}$, respectively). These observations are in line with less electron-donating systems and still provide a red shift due to the methoxy or hydroxyl substituent. The additional absorption band at ~410 nm seen in symmetric ADPM **1**, **2** and **8** was also noticeable in asymmetrical adducts **4** and **6** bearing the hydroxyl substituent. In contrast, ADPM **5** with the methoxy substituent present a relatively smaller band similar to reference **7**.

Electrochemistry

The gathering of information concerning the energy levels of tetradentate ADPM chromophores **1** – **6** and their potential metallic complexes is essential for further integration in various photoactive materials. While optical properties such as absorption and emission can indicate the energy difference between the HOMO and LUMO, only electrochemistry is able to further provide their exact energy level in the ground state. This is especially relevant for a fine-tuning of the properties in given applications. For instance, a mismatch between the LUMO levels of the donor and the acceptor molecules in dye-sensitized solar cells (DSSC) or organic photovoltaic (OPV) devices would not allow efficient electron transfer upon photoexcitation.[2a, 32] Similarly, a high-lying HOMO level might oxidize air-exposed photovoltaic devices or fluorescent sensors in biological environments.[3a, 33] Applications in photocatalysis and electrogenerated chemiluminescence also need insights provided by electrochemistry.[6c, 34] In this

study, the effect of tetradentate motif in ADPM **1** – **6** was compared by cyclic and differential pulse voltammetry techniques (CV and DPV, respectively) to corresponding bidentate derivatives **7** and **8** (Table 2 and SI). These empirical techniques afforded critical information concerning electronic processes and exact energies associated with their HOMO / LUMO states that can further be rationalized with the computational modelization study made (Table 3 and Figure 4).

Table 2 – Electrochemical data for ADPM derivatives **1** – **8** in CH_2Cl_2.

	$E_{1/2}(Ox)$ [a]			$E_{1/2}(Red)$ [a]		
1[b]	1.38[c]	1.06[c]	0.92[c]	-0.78 (123)	-1.40 (149)	---
2	---	1.33[c]	0.75[c]	-0.60[c]	-0.86[c]	-1.05[c, d]
3	1.16[c, e]	1.04[c]	0.66[c]	-0.72 (156)	-0.87[c]	-1.32[c, f]
4	1.29[c, g]	1.14[c]	0.88[c]	-0.78[c]	-1.22 (140)	-1.68
5	---	1.20[c]	0.94[c]	-0.82 (146)	-1.32 (109)	-1.44
6	1.26[c]	1.00[c]	0.83[c]	-0.72[c]	-1.12 (141)	-1.59
7	---	1.36	1.01 (91)	-0.78 (72)	-1.45 (16)	---
8	1.30[c]	1.10[c]	0.71 (61)	-0.92 (106)	-1.52 (193)	---

a) Potentials are in volts vs SCE for CH_2Cl_2deaerated solutions, 0.1 M of TBAP, recorded at 25 ± 1 °C at a sweep rate of 50 mV/s. The difference between cathodic and anodic peak potentials (mV) is given in parentheses. b) Interactions between compound **1** and ferrocene internal reference was observed. Values are reported without correction. Ferrocene value was measured before and after analysis of the compound to assess there was no drifting of the electrode. c) Irreversible. Determined by differential pulse voltammetry (DPV). d) Additional irreversible oxidation observed at -1.60 V. e) Additional irreversible oxidation observed at 1.36 V. f) Two additional irreversible reductions observed at -1.77 and -1.84 V. g) Additional irreversible oxidation was observed at 1.41 V.

Table 3 – HOMO / LUMO levels (in eV) as determined by electrochemistry in CH_2Cl_2 and theoretical calculation along with corresponding ΔE for ADPM derivatives **1** – **8**.

	HOMO Redox	LUMO Redox	ΔE_{Redox} [a)]	HOMO Theo [b)]	LUMO Theo [b)]	ΔE_{Theo} [a)]	ΔE_{Opt} [d)]
1	-5.87	-4.16	1.71	-5.45	-2.88	2.57	1.86
2	-5.70	-4.35	1.35	-5.67	-3.13	2.54	1.88
3	-5.61	-4.22	1.39	-5.74	-3.15	2.59	1.93
4	-5.82	-4.16	1.66	-5.52	-3.03	2.49	1.85
5	-5.89	-4.13	1.76	-5.58	-3.06	2.52	1.89
6	-5.77	-4.23	1.54	-5.59	-3.06	2.53	1.92
7	-5.95 [c)]	-4.17 [c)]	1.78	-5.62	-3.05	2.57	1.92
8	-5.66 [c)]	-4.03 [c)]	1.63	-5.23	-2.81	2.42	1.82

a) Energetic difference (ΔE, in eV) between the HOMO and the LUMO. b) Obtained by theoretical calculation (r-pbe0 / 6-311g(2d,p)) using the CPCM = CH_2Cl_2 polarizable conductor calculation model. c) Obtained from previous work.[10a] d) ΔE qualitatively obtained from the red end of the Gaussian peak of the $\lambda_{max\ red}$ in DCM solution and converted in eV using the formula $E = hc / \lambda$.

Figure 4 – Representation of HOMO / LUMO energy levels (in eV) of ADPM derivatives **1** – **8** as obtained by electrochemistry (black) and DFT calculations (red) along with their associated band-gaps (ΔE in eV; bottom values).

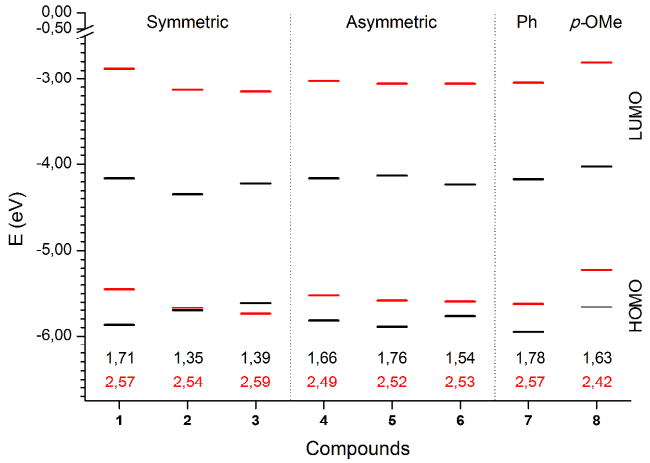

An overview of the electrochemical data for tetradentate ADPMs **1** – **6** (Table 2) suggests a relatively lower stability to oxidation in dichloromethane solution compared to the reference tetraphenyl ADPM **7**. It can be observed that both the first and second oxidation processes are irreversible plus at lower potential in all tetradentate derivatives when compared to the reference, where «pseudoreversible» one-electron processes occur at 1.01 (91) and 1.36 (137) V (mV) vs SCE. In fact, the first oxidation range from 0.66 V for the symmetric ADPM **3** up to 0.94 V for asymmetric ADPM **5** and the second oxidation from 1.00 V for asymmetric derivative **6** up to 1.33 V in the case of the symmetric **2**. In addition, decomposition still appears when a third process is implied (ADPM **1** [1.38 V], **3** [1.16 V], **4** [1.29 V] and **6** [1.26 V]). As a comparison, the electron-rich *para*-methoxyphenyl ADPM **8** showed a pseudoreversible first oxidation at 0.71 (61) V (mV), while instability arises for the second and third ones [1.10 and 1.30 V, respectively]. Irreversible redox processes encountered in substituted ADPM derivatives might be the result of secondary reactions arising in their oxidized forms and are of concern for integration as light-harvesting or life science system components since they are more likely to decompose over time in such environment.[3a, 32a, 35] It is noteworthy that previous work has shown that further coordination of ADPM chromophores onto various metallic centers (e.g. Co^{II}, Ni^{II}, Zn^{II} and Ir^{III}) or the metalloid borane tends to stabilize oxidation processes, therefore improving their potential for such applications.[9a, c, 10a, i, j]

The situation is slightly different for reduction processes, where ADPM **1** and **5** that bear at least one methoxy group can stabilize in pseudoreversible fashion electrons added. Two processes are observed for ADPM **1** [-0.78 (123) and -1.40 (149) V (mV)] and three in the case of **5** [-0.82 (146), -1.32 (109) and -1.44 (122) V (mV)]. These derivatives behave similarly to the reference **7** [-0.78 (72) and -1.45 (16) V (mV)] and the corresponding tetra-methoxy ADPM **8** [-0.92 (106) and -1.52 (193) V (mV)]. The hydroxyl-substituted ADPM **2** presents three

irreversible reductions [-0.60, -0.86 and -1.05 V], while ADPM **3** bearing electron-poor 2-pyridyl proximal substituents has a first pseudoreversible reduction at -0.72 (156) V (mV) and two other ones that are irreversibles at -0.87 and -1.32 V. On the contrary, ADPMs **4** and **6** both present a first reduction that is irreversible, while their second and third ones are pseudoreversibles [-0.78, -1.22 (140) and -1.68 (135) V (mV) for **4**; -0.72, -1.12 (141) and -1.59 (132) for **6**]. From these findings, it appears that derivatives bearing a proximal hydroxyl substituent (ADPM **2**, **4** and **6**) tend to have an irreversible first reduction process. On the other hand, reduction processes implying the methoxy and / or 2-pyridyl moieties present a reversible character. In addition, the presence of two *ortho*-methoxyphenyl groups in proximal positions encountered in ADPM **1** led to easier reductions processes than in the corresponding tetra-methoxy derivative **8**, as can be expected by less electron density present in the former case. Further insights on the molecular orbitals (MOs) implied in the various redox processes can be obtained by analysis of the electron density map provided by computational modelization, which will be discussed in the corresponding section.

Once converted in eV, the potentials of HOMO and LUMO obtained (Table 3) are relevant for a better understanding of the structure – property relationship uniting ADPM **1** – **8** and fine-tuning their incorporation in many applications. The HOMO level increases in the series of symmetric ADPMs **1** to **3** (Figure 4). This behavior seems counterintuitive based solely on the Hammett parameter analysis made before, since the latter, which bears 2-pyridyl proximal rings, should be the hardest to oxidize in the triad. This theoretical assumption is further supported by computational modelization (Figure 4). However, the instability of ADPM **3** observed during the synthesis tends to explain the empirical results obtained by electrochemistry. In the case of ADPM **1** and **2**, the expected trend is respected between the two since the presence of two electron-rich hydroxyl groups in **2** lead to an oxidation potential that is +0.17 eV more positive as

compared to **1** (-5.70 vs -5.87 eV, respectively). Still, the bidentate ADPM **8** bearing four electron-rich –OMe groups remains the easiest to oxidize at -5.66 eV while the tetraphenyl reference compound **7** is the hardest of the series at -5.95 eV. On their side, the asymmetric derivatives **4** to **6** exhibit interesting synergetic effects, with their HOMO levels staying within the range observed for their symmetric counterparts. ADPM **4** with one methoxy and one hydroxyl substituent groups have an HOMO located at -5.82 eV, in between the one of ADPM **1** and **2**. ADPM **5** with an *ortho*-methoxy group and a 2-pyridyl moiety is slightly harder to oxidize with a HOMO at -5.89 eV. While **4** should theoretically present the easiest oxidation of the asymmetric derivatives series due to the presence of two electron-donor substituents, it is ADPM **6** with the hydroxyl group and a 2-pyridyl moiety that happens to be with a HOMO at -5.77 eV. This odd behavior might be attributable to similar oxidation instability as it was observed for ADPM **3**.

Even though the first reduction potential obtained doesn't formally refer to the calculated LUMO energy level of a molecule, it still represents the ability of a molecule to stabilize a negative charge and therefore provides a first approximation of the LUMO's tendency in a series. One observation that can be made from the first reduction process in the series is that *ortho*-methoxy substituents in proximal position appears to have little effect on the LUMO position (-4.16 eV for ADPM **1** and **4**; -4.13 eV for ADPM **5**) as compared to the reference compound **7** (-4.17 eV). This observation suggests the reduction is happening far apart from the proximal moiety when a methoxy substituent is present. This is especially true when considering that ADPM **8** bearing *p*-methoxy groups (including two on the distal rings) was the harder to reduce at -4.03 eV. The presence of 2-pyridyl moieties makes the reduction process easier as can be expected from an electron-poor moiety, with empirical LUMO lying at -4.22 eV for ADPM **3** and -4.23 eV for ADPM **6**. Finally, the relatively easy reduction at -4.35 eV encountered in ADPM **2**

appears to result from instability of the dye since an irreversible peak was observed (Figures S.14 and S.15). As mentioned previously, introduction of a hydroxyl substituent led to such irreversibility for tetradentate derivatives **4** and **6** as well.

The combination of substituent effects on the HOMO and LUMO of tetradentate derivatives led to redox band-gaps (ΔE_{Redox}) ranging from 1.35 eV for symmetric ADPM **2** up to 1.76 eV for asymmetric ADPM **5**. Thus, a fine-tuning of up to 0.41 eV can therefore be achieved in the tetradentate ADPM series presented herein. As compared, a smaller variation of 0.15 eV was observed between the reference compound **7** (1.78 eV) and the electron-rich ADPM **8** equipped of four *p*-methoxy substituents (1.63 eV). Overall, electrochemistry revealed that an accurate control on the energy levels could be achieved through careful selection of the substituents nature, position and combination in ADPM derivatives.

Computational Modelization

DFT analysis

Computational modelization is a highly valuable tool to provide theoretical information at the molecular scale on relative energy levels, electronic distribution in molecular orbitals (MOs), absorption transitions and many other important physical properties such as electron transport within a family of derivatives.[36] Great insights have been provided lately for applications in OPV, DSSC and more broadly speaking for molecular design of organic chromophores with specific UV-vis to NIR absorption and emission properties.[37] Fortunately, systematic computational modelization and benchmarks have already been achieved for BF_2-chelated BODIPY and Aza-BODIPY derivatives in order to establish a general and validated procedure.[20, 38]

DFT results obtained for the ADPM series investigated herein revealed interesting information on their relative HOMO / LUMO energy levels (Figure 4; Figure S.24 of SI) and associated electron distribution (Figures 5 and 6; Table S.1 of SI). The theoretical band gap ($\Delta E_{\text{Theo DFT}}$) ranges from 2.42 to 2.59 eV (Table 3), however, these values are considerably overvalued compared to empirical electrochemistry results (ΔE_{Redox} = 1.35 – 1.78 eV) rendering them difficult to compare directly. As mentioned previously, this is mainly due to the first reduction process probed by electrochemistry being different from the LUMO energy level calculated by DFT and to the instability observed in the tetradentate ADPM series. It is worth noting that the overall match is better when comparing $\Delta E_{\text{Theo DFT}}$ with optical band-gaps (ΔE_{Opt} = 1.82 – 1.96 eV) (Table 3), which are in line with the stability of the dyes observed by photophysical characterization.

Figure 5 – Division of ADPM chromophore for computational modelization analysis

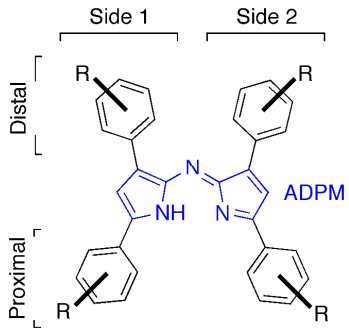

Figure 6 – Representation of HOMO and LUMO of ADPM derivatives **1** – **8** as obtained by DFT computational modelization (Isovalue = 0.02)

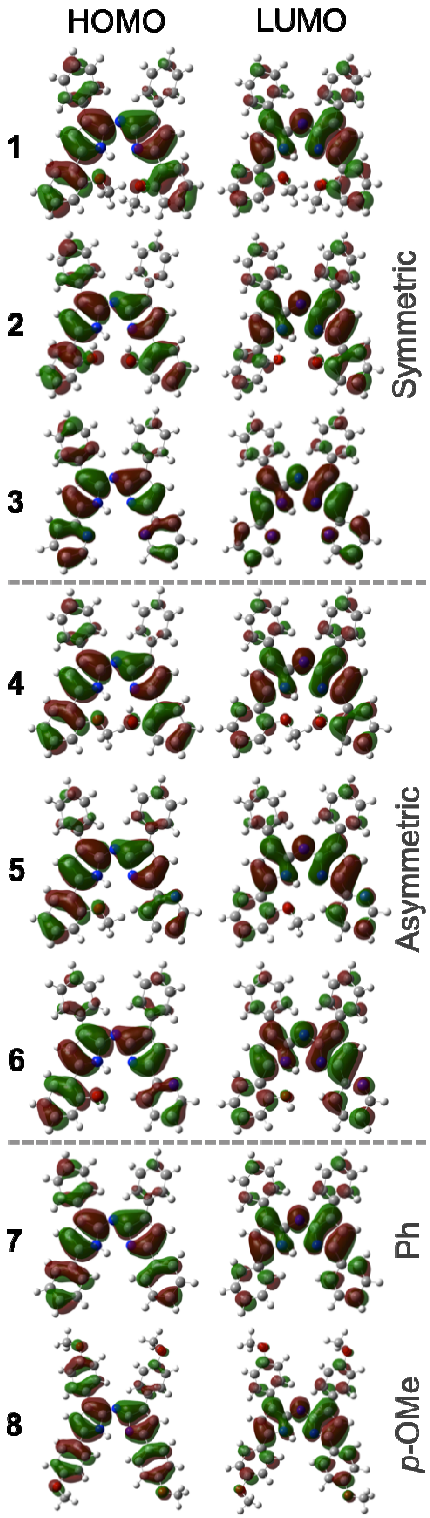

For reference compound **7**, the HOMO calculated at -5.62 eV is mainly centered on the dipyrrolic moiety (ADPM; 66 % of the electronic distribution) and to a lesser extent on the two proximal phenyls (13 % for proximal aryl 1 and 9 % for proximal aryl 2). The LUMO evaluated at -3.05 eV has less ADPM character (63 %), and therefore, transfers less of its electronic density toward proximal aryl 2 (from 9% in the HOMO up to 14%). Similarly, the three other phenyl groups have each 1% less to contribute to this reorganization. The effect of bearing four *para*-methoxyphenyl substituents in ADPM **8** appears to be a marked increase of +0.39 eV for HOMO level (-5.23 eV) and a +0.24 eV change for the LUMO (-2.81 eV), which corresponds to the relative trends observed by electrochemistry (+ 0.29 eV and + 0.14 eV, respectively; Table 3). In this latter symmetric derivative, the electron density of the HOMO is clearly decreased from the ADPM moiety (54 %) as compared to reference **7**, as a result of the four electron-rich substituents' contribution. On the other hand, the LUMO appears to be similarly divided on the substituents, with a small diminution of 2% on the ADPM moiety (61 %) compared to the reference. From these insights, it appears that the first oxidation process observed by electrochemistry for **7** and **8** is most probably based on the ADPM moiety, and it is more affected by the proximal substituents than the distal ones. This last observation is truly stimulating as it provides an additional argument for the exploration of the tetradentate motif as a mean to shift the absorption of ADPMs toward the NIR. The first reduction process should accommodate an additional electron on the distal substituents since the electron density is at the lowest on these positions (about 6% in both derivatives). Another interesting observation to be made is that the HOMO's electronic distribution in both derivatives tends to avoid the bridging nitrogen of the dipyrrolic moiety, dividing the π-system of the chromophore into two sides each including a pyrrole with its proximal and distal aromatic substituents. Instead, it appears the LUMO have a restored delocalization throughout the ADPM moiety, even though the overall electronic

distribution tends to be more equilibrated with the transfer of density toward the peripheral substituents. These observations are in line with the modelization results obtained for similar Aza-BODIPYs systems. For example, Russo *et al.* looked at derivatives bearing four phenyls and *para*-methoxyphenyl substituents in proximal or distal positions.[39] They found a similar behavior of electronic distribution in their symmetric derivatives. The group of Jacquemin obtained results consistent with those of Russo when comparing the frontier orbitals of an Aza-BODIPY bearing para-dimethylaminophenyl electron-donating substituents linked through an alkyne on the proximal phenyls.[20] Kobayashi *et al.* also made a direct comparison by computational modelization between a benzo-fused ADPM derivative and its BF_2-chelated counterpart that revealed a high similarity in the electronic distribution between corresponding HOMOs and LUMOs.[40] This latter example demonstrates the utility of comparing ADPM frontier orbitals with their Aza-BODIPY derivatives and also supports the validity of using a similar computational approach. Finally, the computational results reported lately by Sauvé and coworkers at a lower level of theory for the reference ADPM **7** (PBE0/6-31G(d,p) in gas phase, i.e. no PCM; HOMO = -4.63 eV; LUMO = -3.29 eV; $\Delta E_{\text{Theo DFT}}$ = 1.33 eV)[41] reveals that the computational procedure used herein provides a better fit of about 1 eV for the HOMO (-5.62 eV calculated; -5.95 eV empirical).[42]

A visual overview of the symmetric tetradentate ADPM **1** – **3** (Figure 6) reveals very similar electronic distribution as compared to symmetric references **7** and **8**, where the ADPM moiety and the proximal aryls concentrate most of the density. This is further supported by the values of electronic distribution reported in Table S.1. The presence of two *ortho*-methoxyphenyl substituents in ADPM **1** provides a HOMO resting at -5.45 eV, in between the two bidentate references. The electronic distribution analysis proved that the density is again transferred from the ADPM moiety (62%) to the proximal substituents (17% for proximal 1 and 11% for proximal

2) as compared to **7**. Essentially, the effect of *ortho*-methoxy substituents on the proximal positions of **1** appears to be similar to the one encountered for the *para*-methoxyphenyl in ADPM **8** (17% for proximal 1 and 12% for proximal 2), while the distal phenyls have a similar density to reference **7**. The theoretical LUMO lying at -2.88 eV is also in accordance with the two ADPMs of reference. The only difference is found in the electronic distribution, where the ADPM moiety of **1** (66 %; +3 % vs ADPM **7**) is affected by the presence of methoxy substituents in an opposite fashion than that observed for **8** (61 %; -2 % vs **7**). In fact, this increased of density on the central moiety in ADPM **1** comes from the diminution found on the proximal aryl 1 substituent (8 %) as compared to reference **7** (12 %), a situation not observed in the *para*-substituted **8** (12 %).

ADPM **2** bearing *ortho*-hydroxyl groups present a calculated HOMO at -5.67 eV, lower than its methoxy counterpart ADPM **1**. This finding is in direct opposition with the Hammett parameter analysis and the electrochemical trend observed, where the first oxidation was 0.17 eV less positive (refer to Table 3). In fact, variations of electronic distribution on the ADPM moiety as compared to reference **7** between the tetradentate ADPM **1** (62%; -4 % vs **7**) and **2** (59%; -7 % vs **7**) is consistent with what should be expected from their relative electron-donating ability. However, the principal difference that explains this trend seems to be a better repartition between the two proximal groups in ADPM **2** (15 % for proximal aryl 1 and 16 % for proximal aryl 2). For instance, ADPM **1** had a distribution of 17% on proximal 1 and 11% on proximal 2, while reference **7** was at 13% and 9%, respectively. The LUMO at -3.13 eV present an electronic distribution very similar to ADPM **1**, even though it should lie at higher energy due to the electron-rich character of hydroxyl substituents.

As for symmetric tetradentate ADPM **3**, the observed trends are reversed due to the presence of electron-poor 2-pyridyl moieties. The theoretical HOMO, lying at -5.74 eV, is the lower of the symmetric derivatives as can be expected. The composition of this MO has an enriched electron

density on the ADPM moiety (68 %; +2 % vs **7**) while the proximal substituents both decreased by 1% compared to the tetraphenyl reference. In the same vein, the LUMO at -3.15 eV is the easier to reduce. The electronic distribution of that MO is mainly centered on the ADPM moiety (70 %; +7 % vs **7**), with a lower density on both proximal 2-pyridyl moieties (7 and 11 %, respectively; -5 and -3% vs **7**). From this last observation, it can be proposed with confidence that the first reduction process observed empirically should imply the pyridine rings.

With the analysis of symmetric derivatives in hand, the asymmetry encountered in tetradentate ADPM **4** – **6** ought to reveal interesting features, such as which substituent tends to affect a given frontier MO more. A look at the MO shapes in those derivatives appears to follow the general trends observed previously (Figure 6), i.e., a HOMO divided in two with no conjugation on the bridge of the ADPM moiety, while the LUMO restores the bridging conjugation. The tetradentate ADPM **4** bearing the two electron-donor groups studied herein has a calculated HOMO lying at -5.52 eV, in between its two corresponding symmetric derivatives **1** (-5.45 eV) and **2** (-5.67 eV) albeit being closer to the former. This is of interest since Hammett parameter analysis would suggest a higher character arising from the hydroxyl substituent to influence the first oxidation. Interestingly, one can rationalize that the methoxy group is attached to the "dominant" side 1, where the electronic density is concentrated and tends to be better delocalized throughout as opposed to side 2. This can be expressed by the fact proximal aryl 1 position is holding 17% of the density, the exact same amount found in ADPM **1**, while the hydroxyl group on proximal aryl 2 is at 14% and the ADPM moiety as a whole at 60%. Therefore, it can be considered that the *ortho*-methoxy substituent is dictating the nature of the HOMO. This is in good agreement with the empirical value obtained where the HOMO was at -5.82 eV, closer to the methoxy derivative **1** (-5.87 eV) than the hydroxyl derivative **2** (-5.70 eV). For the LUMO calculated at -3.03 eV, the situation appears to be reversed since it lies closer to the hydroxyl symmetric counterpart **2** (-3.13

eV) than the methoxy derivative **1** (-2.88 eV). However, it is difficult to draw any clear trend from the electronic distribution since it is very similar for the two symmetric derivatives. Similarly, the electrochemical data reveals a first reduction for ADPM **4** at the exact same levels as **1** (-4.16 eV) that should indicate a methoxy-based LUMO, but the irreversibility of the process as encountered in all the hydroxyl derivatives recluses the MO assignment. When introducing a 2-pyridyl moiety in the system (ADPM **5** and **6**), calculated data tend to demonstrate that electronic distribution is mainly affected by this substituent, i.e., the effect of a methoxy or hydroxyl substituent is virtually equivalent. For instance, the calculated HOMO of ADPM **5** is lying at -5.58 eV, close to the -5.59 eV of ADPM **6**. Likewise, the LUMO of both adducts is at -3.06 eV and the exact same electronic distribution is found (ADPM moiety at 67%, proximal aryl 1 bearing the electron-rich substituent at 8% and proximal aryl 2 bearing the pyridyl at 11%). In this situation, calculations appear to be offset when compared to the electrochemical data, but the instability observed in solution again makes it difficult to draw direct conclusions other than the 2-pyridyl substituents having a dominant effect on frontier MOs.

Globally, the DFT modelization of tetradentate ADPM derivatives show that factors other than the classical Hammett parameter might be necessary to fully rationalize trends encountered in the series. Therefore, one still needs to consider insights provided by computational modelization, electrochemistry and structural analysis in order to have a complete representation of a given class of ADPMs and to further fine-tune their properties in a logical manner.

TD-DFT analysis

A systematic TD-DFT analysis of ADPM chromophores is reported here for the first time using TD-BMK/6-311+G(2d,p). Calculated optical absorption bands, oscillator strengths (osc. strengths) and orbitals implied in the excitation for derivatives **1** – **8** are summarized in Tables S.2 – S.9 of SI. Assignment of the transition origin was further made based on this latter information in order to assess the effect of the various substituents studied herein. Figures S.25 – S.32 (see SI) present a superposition of the experimental spectrum obtained in dichloromethane solution and the calculated bands. At first glance, there is a very good correlation between the calculated transitions and empirical observations, which is very promising for *in silico* investigations of potential new ADPMs before their actual synthesis. The relative order of the $\lambda_{max\ red\ Theo}$ for the compounds fully respect the trend observed by UV-vis spectroscopy. A theoretical range of 547 nm for the electron-poor ADPM **3** up to 587 nm for the electron-rich ADPM **8** is found, which tends to underestimate the empirical results ($\lambda_{max\ red}$ ranging from 590 for **3** up to 627 nm for **8**, Table 1). This offset may vary between 34 and 55 nm from the experimental results, depending on the substituents involved and the shape of the absorption spectrum. Slight shifts obtained for the transition energies calculated by TD-DFT can be attributed to the use of a simple solvent model, i.e. no corrections beyond linear-response, and the use of vertical transition that neglect the vibronic effects.[43] The methodology outlined herein is based on the work of Jacquemin *et al.*, who previously benchmarked his work for $-BF_2^+$ chelated aza-BODIPYs.[20]

Looking more specifically at tetraphenyl reference **7**, the calculated transition at 551 nm (osc. strength = 0.885) corresponds to the observed $\lambda_{max\ red}$ = 590 nm, a difference of -39 nm. As can be expected, this excitation is evaluated to be at 99% a HOMO to LUMO (H -> L) transition

where the electronic density on the side 1 of the chromophore is transferred toward the side 2 and the ADPM moiety (refer to Figure 5). In comparison, ADPM **8** has a calculated transition at 587 nm (0.889) that corresponds to $\lambda_{max\ red}$ = 627 nm, a difference of -40 nm that is similar to what was observed for **7**. This 99% H -> L transition takes the density of three peripheral *p*-methoxyphenyl substituents toward the distal 2 substituent and ADPM moiety.

The analysis of tetradentate ADPM **1** – **6** show the H -> L transition to be characteristic of every $\lambda_{max\ red}$ transition observed (99 %), as expected. Based on this unambiguous behavior throughout the series and our main interest toward $\lambda_{max\ red}$ from a light-harvesting point of view, we used a simple MO analysis method rather than the difference density plot or the more advanced concept of natural transition orbitals (NTO).[44] While these two last analysis methods can help represents transitions when a high degree of orbital mixing is obtained from the TD-DFT calculations,[43] no such mixing was found herein and the MO analysis method therefore appears faster and equally satisfactory to represent the $\lambda_{max\ red}$ transitions. The symmetric derivatives **1** and **2,** having electron density transferred from the conjugated side 1 toward the ADPM moiety, differ from the electron-poor 2-pyridyl derivative **3,** where the transfer is additionally delocalized over the rest of side 2. Interestingly, TD-DFT results are in good agreement with the Hammett parameter trend as the calculated transition of hydroxyl-substituted **2** at 560 nm (0.834) shows a plus 9 nm difference compared to reference **7**, while methoxy bearing ADPM **1** transition found at 553 nm (0.834) is only plus 2 nm. Similarly, ADPM **3** with electron-withdrawing substituents is calculated at 547 nm (0.877), a minus 4 nm hypsochromic difference. When asymmetry is introduced, both substituents contribute to the $\lambda_{max\ red\ Theo}$. ADPM **4** has a calculated transition at 571 nm (0.861). This is a +20 nm difference compared to **7** arising from a synergetic effect of the methoxy and hydroxyl proximal substituents, i.e. the difference is twice as high as the sum of their individual contributions found previously in symmetric

derivatives. This behavior might be attributable to a push-pull effect, especially when looking at the introduction of the electron-withdrawing 2-pyridyl moiety in ADPM **5** and **6**. In these latter derivatives, the donor substituent involved transfers the electronic density toward the side bearing the 2-pyridyl group in addition to the ADPM moiety. In this way, the calculated difference still stands at plus 15 nm for adduct **5** and plus 13 nm for **6**.

The observed $\lambda_{max\ violet}$ prominent in compounds bearing methoxy or hydroxyl substituents, including *para*-substituted ADPM **8**, attracted our attention since it represents an efficient way to improve the overall panchromaticity of ADPM chromophores for light-harvesting applications. Maxima of this new absorption band range between 407 nm for **1** and 418 nm for **6**, with extinction coefficients (ε) evaluated at 3.9 – 10 x 10^3 $M^{-1}cm^{-1}$ for the series. The systematic assignation of the excitation calculated by TD-DFT to their corresponding observed absorption band was used to unravel origin of this band (Tables S.2 – S.9). First looking at the reference, tetraphenyl ADPM **7** present more or less a plateau in the 370 – 430 nm spectrum region, with an ε ~ 3.75 x 10^{-3} $M^{-1}cm^{-1}$. Two calculated transitions are found in this range at 372 nm (osc. strength = 0.190) and 428 nm (0.059) to explain the non-zero absorption. They are, respectively, H-2 -> L (97%) and H-1 -> L (96%) excitations taking the electronic density from the distal 1 and 2 phenyls toward their proximal counterparts and the ADPM moiety. Careful analysis of the data revealed the apparition of $\lambda_{max\ violet}$ in ADPMs **1**, **2**, **4** – **6** and **8** is attributable in each case to a significant increase in the oscillator strength of at least one of these two transitions (up to 249% compared to **7**). In addition, a new transition is found in all these derivatives implying electronic transfer from the peripheral substituents toward the ADPM moiety upon photoexcitation. On the other hand, the ADPM **3** with 2-pyridyl proximal substituents with no observed $\lambda_{max\ violet}$ have only two calculated transitions at 381 nm (0.164) and 441 nm (0.064). These transitions are bathochromically shifted compared to reference **7**, as can be expected from the electron-

withdrawing effect, but with similar intensity of oscillator strengths (86% and 108% of the reference value, respectively).

X-Ray Diffraction

Crystals suitable for X-ray diffraction studies were obtained for compounds **1**, **3**, **4** and **5**.[45] Solid-state structure and refinement data are presented in figures 7 – 8 and SI. All the four compounds crystallized in the monoclinic crystal system, space groups: $P2_1/n$, $P2_1$, Pc, and $P2_1/c$, respectively (Table S.10). For ADPM **3**, only isotropic refinement of the structure was performed due to poor crystal quality and only the connectivity of the atoms is discussed herein (Figure 7 bottom; see SI for more details). However, the identity of this last compound was further confirmed by mass spectrometry performed on the same crystal sample (see experimental section).

For compounds **1**, **4** and **5**, an analysis of bond lengths in the ADPM unit (Table S.11) confirms the conjugated nature of this moiety, as found for similar compounds.[10a, 12] In addition, the observed planarity of the central pyrrolic rings is another common feature of the ADPM derivatives.[10a, 10c] The tilt angle between the planes of the central pyrrolic rings is 1.3(1)° in ADPM **8** bearing *para*- substituents on the aryl rings.[10a] In comparison, compounds **1**, **4**, and **5** all featuring *ortho*- substituted proximal aryl rings present slight deviations from planarity of the pyrrolic rings, with values for corresponding tilt angles of 10.9(1)°, 8.0(1)°, and 9.8(1)°, respectively (Table S.11).

Conventional H-bonding and weak H-bonding (intramolecular and intermolecular), together with π – π and π – H-D (D = C(sp2), N, O) interactions can be identified as packing forces in the three structures. The intramolecular H-bonding patterns in **1**, **4**, and **5** are represented in figures 7 and 8. The analysis of the corresponding numeric values (Table S.12) show conventional and

weak H-bonds.[46] A 3-center bifurcated H-bonding pattern (N1—H1···O1 and N1—H1···N3) is observed for each of the three structures.[47]

The orientation of aryl rings with respect to the ADPM moiety is dictated by the steric tension induced in the substitution pattern, as well as attractive and repulsive intramolecular and intermolecular H-bonding and π – π interactions. Values of the tilt angles between the plane of the ADPM moiety and the plane of the aryl rings are shown in the SI (Table S.11). As a general observation, the proximal aryl rings are less tilted with respect to the ADPM plane than the distal ones for the three structures (with one exception: Ar_1 and Ar_2 in compound **1** – see Figure 1 for the nomenclature). The position of the *ortho* substituents on the proximal aryl rings is endo (Ar_1) / exo (Ar_4) in case of **1** and **5**, and becomes endo (Ar_1) / endo (Ar_4) for compound **4**, most probably due to the extended H-bonding pattern specific to **4** (Figures 8 and S.33). The 'opening' angles of the ADPM moiety (i.e. C1-N2-C17, N1-C1-N2 and N2-C17-N3) are higher in this last compound, as can be expected from the more sterically hindered conformation (Table S.11).

Compound **4** crystallized with four molecules in the asymmetric unit showing similar conformations, bond lengths and angles. The proximal aryl substituents and the ADPM moiety are very close to planarity, with values for the tilt angles between the corresponding planes ranging between 1.2(1) – 4.2(1)°. The only notable difference among the four molecules is observed at the level of distal aryl rings, which present different orientations maximizing the π – H-C(sp^2) intermolecular interactions between two adjacent molecules (Figure S.33).

The enhanced rigidity obtained by the specific intramolecular H-bonding pattern, the global planarity in the molecule and the stronger π – π and π – H-C(sp^2) interactions can all be related to the photophysical properties of the system. For example, red-shifted maxima and higher molar absorptivity observed in the absorption properties of compound **4** (see Spectroscopic Properties section) are indicative that these specific interactions can be partially maintained in solution.

Figure 7 – Solid-state structure of symmetric ADPM **1** (top; ellipsoids shown at 50% probability level; intramolecular H-bonds represented in green) and ADPM **3** (bottom; isotropic model).

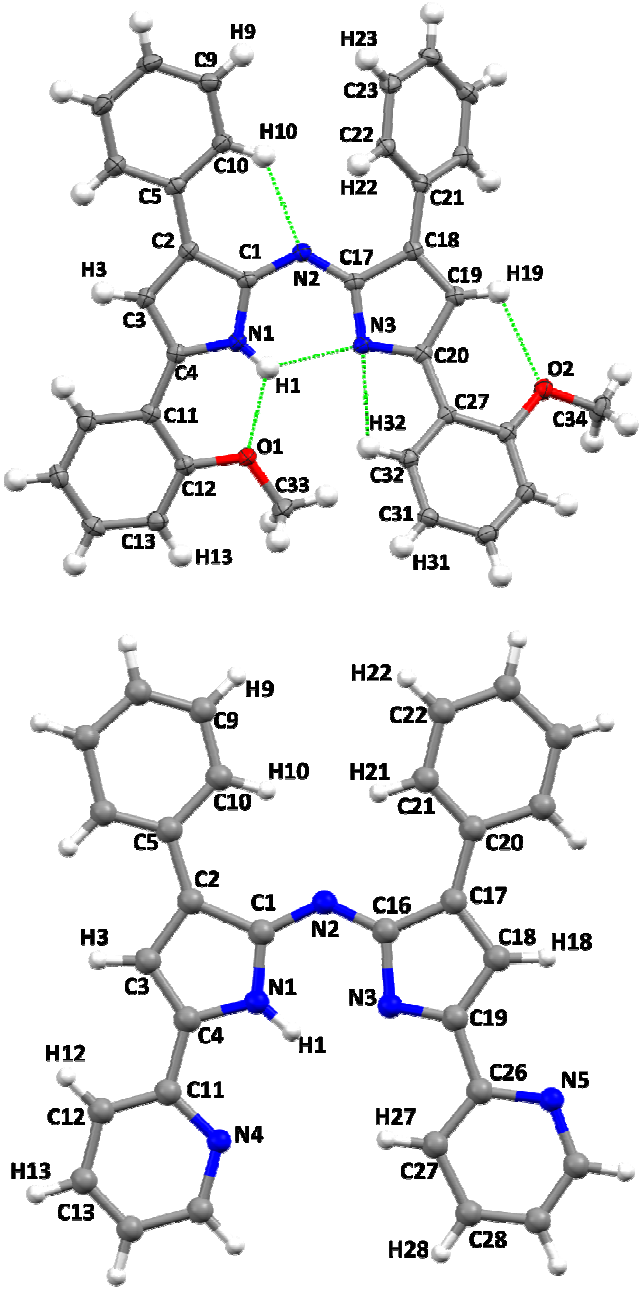

Figure 8 – Solid-state structures of asymmetric ADPM **4** (top; only one of the four molecules in the asymmetric unit is presented) and ADPM **5** (bottom; ellipsoids shown at 50% probability level; intramolecular H-bonds represented in green).

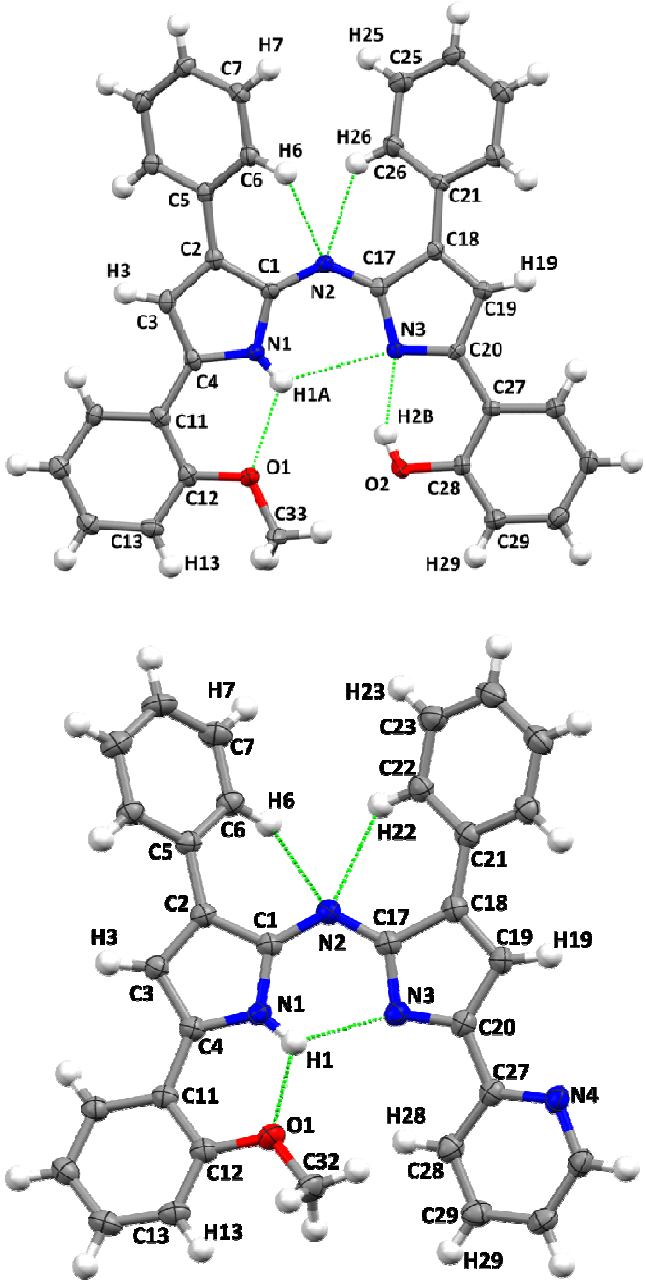

CONCLUSION

In conclusion, the systematic study of symmetric and asymmetric tetradentate ADPM chromophores **1** – **6** was achieved and compared with reference bidentate compounds **7** and **8** in order to gain information on their structure – property relationship. Four of the derivatives have never been reported before and symmetric ADPM **3** represent the first example of 2-pyridyl moieties installed in the proximal position. This comparative investigation was made possible through a new straightforward synthetic approach to access asymmetric derivatives **4** – **6** that avoid the tedious heterocycle formation of nitroso-pyrrole intermediates. Tetradentate ADPMs were studied by UV-vis spectroscopy, revealing the possibility of fine-tuning the absorption maxima from 598 up to 619 nm in the red part of the spectrum and to improve harvesting of violet light (~410 nm) through variation of the proximal substituents combination, although no emission was observed. Further characterization was made by electrochemistry in order to obtain the energy levels of the chromophores, which is crucial for their integration into various photoactive materials. The experimental data showed a tendency for degradation upon redox processes in solution, which might be addressed by coordination of the ligands to metal ions as was previously reported. X-Ray structural analysis was made on previously reported ADPM **1** and newly synthetized ADPM **3** – **5** and these structural data were used for computational modelization of the series. DFT theoretical calculations at the PBE0 / 6-311G(2d,p) level provided information on the factors affecting frontier molecular orbitals and energy levels observed empirically. The TD-DFT protocol used for the first time on ADPM chromophores, TD-BMK/6-311+G(2d,p) (PCM = CH_2Cl_2), was able to establish a good correlation with the observed absorption spectrum and explained the improved absorption of violet light. These

compounds are especially of interest since the tetradentate motifs developed herein allow for a bio-mimicry of metalloporphyrinoids, without the demanding synthesis of the macrocycles. Noteworthy, the π-conjugation extension made possible through metal-mediated planarization should induce bathochromic shift toward the NIR, a critical region for light-harvesting applications. In addition, the coordination mode ranging from XL_3 to X_3L possible with tetradentate ADPM **1** – **6** offers an unsurpassed versatility. From there, multiple applications can be envisioned, varying from light-harvesting / photoactive materials to catalysts, sensors and even beyond.

ASSOCIATED CONTENT

Supporting Information

NMR and HR-ESIMS data for newly synthesized ADPM **3** – **6**; cyclic and differential pulse voltammograms for ADPM **1** – **6**; DFT and TD-DFT computational modelization data for ADPM **1** – **8**; crystal data and details of the structure determination for **1**, **3**, **4** and **5** (CCDC Numbers 1005388 – 1005391) along with packing diagram of **4**.

AUTHOR INFORMATION

Corresponding Author

* E-mail: garry.hanan@umontreal.ca ; Fax: +1 514 343 7586; Tel: +1 514 340 5156.

ACKNOWLEDGEMENTS

GSH thanks the Natural Sciences and Engineering Research Council of Canada, the Centre for Self-Assembled Chemical Structures (CSACS), the Centre in Green Chemistry and Catalysis (CGCC) and the Université de Montréal (UdeM) for financial support. AB is thankful of NSERC, FQRNT and Saint-Jean Photochemicals Inc. (sjpc.com) for funding through a BMP-Innovation grant and to UdeM for an excellence grant. An acknowledgment goes to Compute Canada / Calcul Canada for access through their national supercomputing platform at University of Manitoba's Grex infrastructure supported by Westgrid. AB is grateful to Anne-Catherine Bédard and Daniel Chartrand for useful scientific discussions. The authors are also appreciative to the NMR, Mass Spectroscopy and X-ray laboratories of UdeM plus Prof. Christian Reber for access to his UV/vis instrument.

REFERENCES

1. (a) Rogers, M. A. T., *Nature* **1943,** *151*, 504. (b) Rogers, M. A. T., *J. Chem. Soc.* **1943**, 590-596. (c) Rogers, M. A. T., U.S. Patent 2382914, **1945**.
2. (a) Bessette, A.; Hanan, G. S., *Chem. Soc. Rev.* **2014,** *43*, 3342-3405. (b) Loudet, A.; Burgess, K., *Chem. Rev.* **2007,** *107*, 4891-4932.
3. (a) Boens, N.; Leen, V.; Dehaen, W., *Chem. Soc. Rev.* **2012,** *41*, 1130-1172. (b) Gawley, R. E.; Mao, H.; Haque, M. M.; Thorne, J. B.; Pharr, J. S., *J. Org. Chem.* **2007,** *72*, 2187-2191. (c) Coskun, A.; Yilmaz, M. D.; Akkaya, E. U., *Org. Lett.* **2007,** *9*, 607-609. (d) Jokic, T.; Borisov, S. M.; Saf, R.; Nielsen, D. A.; Kühl, M.; Klimant, I., *Anal. Chem.* **2012,** *84*, 6723-6730.
4. (a) Yuan, L.; Lin, W.; Zheng, K.; He, L.; Huang, W., *Chem. Soc. Rev.* **2013,** *42*, 622-661. (b) Collado, D.; Vida, Y.; Najera, F.; Perez-Inestrosa, E., *RSC Adv.* **2014,** *4*, 2306-2309.
5. (a) Awuah, S. G.; You, Y., *RSC Adv.* **2012,** *2*, 11169-11183. (b) Batat, P.; Cantuel, M.; Jonusauskas, G.; Scarpantonio, L.; Palma, A.; O'Shea, D. F.; McClenaghan, N. D., *J. Phys. Chem. A* **2011,** *115*, 14034 - 14039. (c) Gorman, A.; Killoran, J.; O'Shea, C.; Kenna, T.; Gallagher, W. M.; O'Shea, D. F., *J. Am. Chem. Soc.* **2004,** *126*, 10619-10631.
6. (a) Tanaka, K.; Chujo, Y., *Macromol. Rapid Commun.* **2012,** *33*, 1235-1255. (b) Benstead, M.; Mehl, G. H.; Boyle, R. W., *Tetrahedron* **2011,** *67*, 3573-3601. (c) Nepomnyashchii, A. B.; Bard, A. J., *Acc. Chem. Res.* **2012,** *45*, 1844-1853. (d) Ma, X.; Mao, X.;

Zhang, S.; Huang, X.; Cheng, Y.; Zhu, C., *Polym. Chem.* **2013,** *4*, 520-527. (e) Ma, X.; Jiang, X.; Zhang, S.; Huang, X.; Cheng, Y.; Zhu, C., *Polym. Chem.* **2013,** *4*, 4396-4404.
7. Tekin, S.; Küçüköz, B.; Yılmaz, H.; Sevinç, G.; Hayvalı, M.; Gul Yaglioglu, H.; Elmali, A., *J. Photochem. Photobiol., A* **2013,** *256*, 23-28.
8. (a) Ziessel, R.; Harriman, A., *Chem. Commun.* **2011,** *47*, 611-631. (b) Ziessel, R.; Ulrich, G.; Haefele, A.; Harriman, A., *J. Am. Chem. Soc.* **2013,** *135*, 11330-11344. (c) Lee, C. Y.; Farha, O. K.; Hong, B. J.; Sarjeant, A. A.; Nguyen, S. T.; Hupp, J. T., *J. Am. Chem. Soc.* **2011,** *133*, 15858-15861. (d) Shi, W.-J.; El-Khouly, M. E.; Ohkubo, K.; Fukuzumi, S.; Ng, D. K. P., *Chem. Eur. J.* **2013,** *19*, 11332-11341. (e) D'Souza, F.; Amin, A. N.; El-Khouly, M. E.; Subbaiyan, N. K.; Zandler, M. E.; Fukuzumi, S., *J. Am. Chem. Soc.* **2012,** *134*, 654-664. (f) Yuan, M.; Yin, X.; Zheng, H.; Ouyang, C.; Zuo, Z.; Liu, H.; Li, Y., *Chem. Asian J.* **2009,** *4*, 707-713. (g) Amin, A. N.; El-Khouly, M. E.; Subbaiyan, N. K.; Zandler, M. E.; Fukuzumi, S.; D'Souza, F., *Chem. Commun.* **2012,** *48*, 206-208. (h) Gobeze, H. B.; Bandi, V.; D'Souza, F., *Phys. Chem. Chem. Phys.* **2014,** *16*, 18720-18728.
9. (a) Senevirathna, W.; Sauvé, G., *J. Mater. Chem. C* **2013,** *1*, 6684-6694. (b) Mueller, T.; Gresser, R.; Leo, K.; Riede, M., *Sol. Energy Mater. Sol. Cells* **2012,** *99*, 176-181. (c) Gao, L.; Tang, S.; Zhu, L.; Sauvé, G., *Macromolecules* **2012,** *45*, 7404-7412. (d) Gao, L.; Senevirathna, W.; Sauvé, G. v., *Org. Lett.* **2011,** *13*, 5354-5357. (e) Leblebici, S. Y.; Chen, T. L.; Olalde-Velasco, P.; Yang, W.; Ma, B., *ACS Appl. Mater. Interfaces* **2013,** *5*, 10105-10110. (f) Khan, T. K.; Sheokand, P.; Agarwal, N., *Eur. J. Org. Chem.* **2014**, 1416-1422.
10. (a) Bessette, A.; Ferreira, J. G.; Giguère, M.; Bélanger, F.; Désilets, D.; Hanan, G. S., *Inorg. Chem.* **2012,** *51*, 12132-12141. (b) Sakamoto, R.; Kusaka, S.; Kitagawa, Y.; Kishida, M.-a.; Hayashi, M.; Takara, Y.; Tsuchiya, M.; Kakinuma, J.; Takeda, T.; Hirata, K.; Ogino, T.; Kawahara, K.; Yagi, T.; Ikehira, S.; Nakamura, T.; Isomura, M.; Toyama, M.; Ichikawa, S.; Okumura, M.; Nishihara, H., *Dalton Trans.* **2012,** *41*, 14035-14037. (c) Palma, A.; Gallagher, J. F.; Mueller-Bunz, H.; Wolowska, J.; McInnes, E. J. L.; O'Shea, D. F., *Dalton Trans.* **2009**, 273-279. (d) Teets, T. S.; Partyka, D. V.; Updegraff, J. B.; Gray, T. G., *Inorg. Chem.* **2008,** *47*, 2338-2346. (e) Deligonul, N.; Gray, T. G., *Inorg. Chem.* **2013,** *52*, 13048-13057. (f) Gao, L.; Deligonul, N.; Gray, T. G., *Inorg. Chem.* **2012,** *51*, 7682-7688. (g) Teets, T. S.; Updegraff, J. B., III; Esswein, A. J.; Gray, T. G., *Inorg. Chem.* **2009,** *48*, 8134-8144. (h) Partyka, D. V.; Deligonul, N.; Washington, M. P.; Gray, T. G., *Organometallics* **2009,** *28*, 5837-5840. (i) Deligonul, N.; Browne, A. R.; Golen, J. A.; Rheingold, A. L.; Gray, T. G., *Organometallics* **2014,** *33*, 637-643. (j) Berhe, S. A.; Rodriguez, M. T.; Park, E.; Nesterov, V. N.; Pan, H.; Youngblood, W. J., *Inorg. Chem.* **2014,** *53*, 2346-2348. (k) McLean, T. M.; Telfer, S. G.; Elliott, A. B. S.; Gordon, K. C.; Lein, M.; Waterland, M. R., *Dalton Trans.* **2014**, Advance Article, DOI: 10.1039/C4DT01588F.
11. (a) Zhao, W.; Carreira, E. M., *Chem. - Eur. J.* **2006,** *12*, 7254-7263. (b) Zhao, W.; Carreira, E. M., *Angew. Chem., Int. Ed.* **2005,** *44*, 1677-1679. (c) Wu, Y.; Cheng, C.; Jiao, L.; Yu, C.; Wang, S.; Wei, Y.; Mu, X.; Hao, E., *Org. Lett.* **2014,** *16*, 748-751.
12. Loudet, A.; Bandichhor, R.; Burgess, K.; Palma, A.; McDonnell, S. O.; Hall, M. J.; O'Shea, D. F., *Org. Lett.* **2008,** *10*, 4771-4774.
13. (a) Scholes, G. D.; Fleming, G. R.; Olaya-Castro, A.; van Grondelle, R., *Nat. Chem.* **2011,** *3*, 763-774. (b) Hill, J. P.; D'Souza, F.; Ariga, K., Porphyrinoids: Highly Versatile, Redox-Active Scaffolds for Supramolecular Design and Biomimetic Applications. In *Supramol. Chem.*, John Wiley & Sons, Ltd: 2012. (c) Fukuzumi, S.; Honda, T.; Kojima, T., *Coord. Chem. Rev.* **2012,** *256*, 2488-2502. (d) Nemykin, V. N.; Galloni, P.; Floris, B.; Vecchi, A., *J. Porphyrins Phthalocyanines* **2013,** *17*, 165-196. (e) Li, C.; Ulrich, M.; Liu, X.; Wurst, K.; Muller, T.; Krautler, B., *Chem. Sci.* **2014,** *5*, 3388-3395.

14. (a) Hennessy, E. T.; Betley, T. A., *Science* **2013,** *340*, 591-595. (b) Prier, C. K.; Rankic, D. A.; MacMillan, D. W. C., *Chem. Rev.* **2013,** *113*, 5322-5363. (c) Whiteoak, C. J.; Salassa, G.; Kleij, A. W., *Chem. Soc. Rev.* **2012,** *41*, 622-631. (d) Rausaria, S.; Kamadulski, A.; Rath, N. P.; Bryant, L.; Chen, Z.; Salvemini, D.; Neumann, W. L., *J. Am. Chem. Soc.* **2011,** *133*, 4200-4203.
15. Zhang, X.; Yu, H.; Xiao, Y., *J. Org. Chem.* **2012,** *77*, 669-673.
16. Grossi, M.; Palma, A.; McDonnell, S. O.; Hall, M. J.; Rai, D. K.; Muldoon, J.; O'Shea, D. F., *J. Org. Chem.* **2012,** *77*, 9304-9312.
17. Hall, M. J.; McDonnell, S. O.; Killoran, J.; O'Shea, D. F., *J. Org. Chem.* **2005,** *70*, 5571-5578.
18. In *Comprehensive Heterocyclic Chemistry*, Bird, C. W.; Cheeseman, G. W. H., Eds. Pergamon: Oxford, 1984; Vol. 4, pp 209-210.
19. (a) Loudet, A.; Bandichhor, R.; Wu, L.; Burgess, K., *Tetrahedron* **2008,** *64*, 3642-3654. (b) Buryakovskaya, E. G.; Tsukerman, S. V.; Lavrushkin, V. F., *Russ. J. Phys. Chem.* **1969,** *43*, 477–480.
20. Le Guennic, B.; Maury, O.; Jacquemin, D., *Phys. Chem. Chem. Phys.* **2012,** *14*, 157-164.
21. Frisch, M. J.; Trucks, G. W.; Schlegel, H. B.; Scuseria, G. E.; Robb, M. A.; Cheeseman, J. R.; Scalmani, G.; Barone, V.; Mennucci, B.; Petersson, G. A.; Nakatsuji, H.; Caricato, M.; Li, X.; Hratchian, H. P.; Izmaylov, A. F.; Bloino, J.; Zheng, G.; Sonnenberg, J. L.; Hada, M.; Ehara, M.; Toyota, K.; Fukuda, R.; Hasegawa, J.; Ishida, M.; Nakajima, T.; Honda, Y.; Kitao, O.; Nakai, H.; Vreven, T.; J. A. Montgomery, J.; Peralta, J. E.; Ogliaro, F.; Bearpark, M.; Heyd, J. J.; Brothers, E.; Kudin, K. N.; Staroverov, V. N.; Kobayashi, R.; Normand, J.; Raghavachari, K.; Rendell, A.; Burant, J. C.; Iyengar, S. S.; Tomasi, J.; Cossi, M.; Rega, N.; Millam, J. M.; Klene, M.; Knox, J. E.; Cross, J. B.; Bakken, V.; Adamo, C.; Jaramillo, J.; Gomperts, R.; Stratmann, R. E.; Yazyev, O.; Austin, A. J.; Cammi, R.; Pomelli, C.; Ochterski, J. W.; Martin, R. L.; Morokuma, K.; Zakrzewski, V. G.; Voth, G. A.; Salvador, P.; Dannenberg, J. J.; Dapprich, S.; Daniels, A. D.; Farkas, Ö.; Foresman, J. B.; Ortiz, J. V.; Cioslowski, J.; Fox, D. J. *Gaussian 09 Revision D.01*, Gaussian Inc. Wallingford CT 2009.
22. (a) Perdew, J. P.; Burke, K.; Ernzerhof, M., *Phys. Rev. Lett.* **1996,** *77*, 3865-3868. (b) Perdew, J. P.; Burke, K.; Ernzerhof, M., *Phys. Rev. Lett.* **1997,** *78*, 1396. (c) Adamo, C.; Barone, V., *J. Chem. Phys.* **1999,** *110*, 6158-6169.
23. Tomasi, J.; Mennucci, B.; Cammi, R., *Chem. Rev.* **2005**, 2999-3093.
24. Boese, A. D.; Martin, J. M. L., *J. Chem. Phys.* **2004,** *121*, 3405-3416.
25. Dennington, R.; Keith, T.; Millam, J.; Eppinnett, K.; Hovell, W. L.; Gilliland, R. *GaussView Version 3.09*, Semichem Inc., Shawnee Mission KS, 2003.
26. O'Boyle, N. M.; Tenderholt, A. L.; Langner, K. M., *J. Comp. Chem.* **2008,** *29*, 839-845.
27. Chemissian, a computer program to analyze and visualize quantum-chemical calculations, by L. Skripnikov. For the current version, see http://www.chemissian.com
28. Blay, G.; Incerti, C.; Muñoz, M. C.; Pedro, J. R., *Eur. J. Org. Chem.* **2013**, 1696-1705.
29. Removal of the solvent at 30°C in vacuo led to the discoloration of the solution, i.e. degradation of the chromophore.
30. To note, it was mandatory to solubilize both partner in warm EtOH before adding the ammonium source, otherwise, the undesired formation of the symmetric ADPM 2 resulting from the nitroketone partner was observed to a greater extend.
31. Hansch, C.; Leo, A.; Taft, R. W., *Chem. Rev.* **1991,** *91*, 165-195.
32. (a) Mishra, A.; Bäuerle, P., *Angew. Chem., Int. Ed.* **2012,** *51*, 2020-2067. (b) Li, Y., *Acc. Chem. Res.* **2012,** *45*, 723–733. (c) Kolemen, S.; Bozdemir, O. A.; Cakmak, Y.; Barin, G.; Erten-

Ela, S.; Marszalek, M.; Yum, J.-H.; Zakeeruddin, S. M.; Nazeeruddin, M. K.; Grätzel, M.; Akkaya, E. U., *Chem. Sci.* **2011,** *2*, 949-954.
33. Blouin, N.; Michaud, A.; Gendron, D.; Wakim, S.; Blair, E.; Neagu-Plesu, R.; Belletête, M.; Durocher, G.; Tao, Y.; Leclerc, M., *J. Am. Chem. Soc.* **2008,** *130*, 732-742.
34. Li, W.; Li, L.; Xiao, H.; Qi, R.; Huang, Y.; Xie, Z.; Jing, X.; Zhang, H., *RSC Adv.* **2013,** *3*, 13417-13421.
35. (a) Gendron, D.; Leclerc, M., *Energy Environ. Sci.* **2011,** *4*, 1225-1237. (b) Son, H. J.; Carsten, B.; Jung, I. H.; Yu, L., *Energy Environ. Sci.* **2012,** *5*, 8158-8170.
36. (a) Zhao, Y.; Truhlar, D. G., *Acc. Chem. Res.* **2008,** *41*, 157-167. (b) Geerlings, P.; Fias, S.; Boisdenghien, Z.; De Proft, F., *Chem. Soc. Rev.* **2014**. (c) Yoshizawa, K., *Acc. Chem. Res.* **2012,** *45*, 1612-1621.
37. (a) Hachmann, J.; Olivares-Amaya, R.; Jinich, A.; Appleton, A. L.; Blood-Forsythe, M. A.; Seress, L. R.; Roman-Salgado, C.; Trepte, K.; Atahan-Evrenk, S.; Er, S.; Shrestha, S.; Mondal, R.; Sokolov, A.; Bao, Z.; Aspuru-Guzik, A., *Energy Environ. Sci.* **2014,** *7*, 698-704. (b) Pastore, M.; Fantacci, S.; De Angelis, F., *J. Phys. Chem. C* **2013,** *117*, 3685-3700. (c) Preat, J.; Jacquemin, D.; Perpete, E. A., *Energy Environ. Sci.* **2010,** *3*, 891-904. (d) Liu, X.; Xu, Z.; Cole, J. M., *J. Phys. Chem. C* **2013,** *117*, 16584-16595. (e) Jacquemin, D.; Planchat, A.; Adamo, C.; Mennucci, B., *J. Chem. Theo. Comp.* **2012,** *8*, 2359-2372. (f) Qi, D.; Jiang, J., *J. Phys. Chem. A* **2011,** *115*, 13811-13820. (g) Fabian, J., *Dyes Pigm.* **2010,** *84*, 36-53. (h) Jacquemin, D.; Perpète, E. A.; Ciofini, I.; Adamo, C., *Acc. Chem. Res.* **2009,** *42*, 326-334.
38. (a) Chibani, S.; Le Guennic, B.; Charaf-Eddin, A.; Laurent, A. D.; Jacquemin, D., *Chem. Sci.* **2013,** *4*, 1950-1963. (b) Chibani, S.; Le Guennic, B.; Charaf-Eddin, A.; Maury, O.; Andraud, C.; Jacquemin, D., *J. Chem. Theo. Comp.* **2012**, 3303–3313.
39. Quartarolo, A. D.; Russo, N.; Sicilia, E., *Chem. - Eur. J.* **2006,** *12*, 6797-6803.
40. Lu, H.; Shimizu, S.; Mack, J.; Shen, Z.; Kobayashi, N., *Chem. Asian J.* **2011,** *6*, 1026-1037.
41. Senevirathna, W.; Daddario, C. M.; Sauvé, G., *J. Phys. Chem. Lett.* **2014,** *5*, 935-941.
42. Indeed, one has to keep in mind that formal evaluation of redox properties in solution by computational modelization generally demand, in addition to the geometry optimization of the ground state molecule under a polarization continuum, a look at oxidized and reduced forms in order to account for molecular and solvent reorganization energies. While such a highly demanding procedure tends to be more accurate, the ratter simple DFT procedure PBE0/6-311G(2d,p) with PCM depicted here appears to be a highly valuable tool in order to establish a qualitative structure-property relationship in a series of ADPMs at much lower computational cost. For more details, refer to: (a) Davis et al., *J Phys. Chem. A* **2010**, *114*, 12299-12304; (b) Lynch et al., *J. Org. Chem.* **2012**, *77*, 6423-6430; (c) Mendez-Hernandez et al., *J. Mol. Model.* **2013**, *19*, 2845-2848.
43. Adamo, C.; Jacquemin, D., *Chem. Soc. Rev.* **2013,** *42*, 845-856.
44. (a) Plasser, F.; Wormit, M.; Dreuw, A., *J. Chem. Phys.* **2014,** *141*, 024106. (b) Plasser, F.; Bäppler, S. A.; Wormit, M.; Dreuw, A., *J. Chem. Phys.* **2014,** *141*, 024107.
45. CCDC 1005388-1005391 contains the supplementary crystallographic data for this paper. These data can be obtained free of charge via http://www.ccdc.cam.ac.uk/data_request/cif, or by emailing data_request@ccdc.cam.ac.uk, or by contacting The Cambridge Crystallographic Data Centre, 12, Union Road, Cambridge CB2 1EZ, UK; fax: +44 1223 336033.
46. Desiraju, G. R.; Steiner, T., *The Weak Hydrogen Bond: In Structural Chemistry and Biology*. Oxford University Press: 1999.

47. Jeffrey, G.; Saenger, W., Definitions and Concepts. In *Hydrogen Bonding in Biological Structures*, Springer Berlin Heidelberg: 1991; pp 15-48.